# *Medicago truncatula CORYNE* modulates inflorescence meristem branching, nutrient signaling, and arbuscular mycorrhizal symbiosis

Johnathan Orosz[1], Erica Xinlei Lin[1]*, Yerisf C. Torres Ascurra[3]*, Mikayla Kappes[3]*, Penelope Lindsay[2]*, Sagar Bashyal[1,3,4], Hasani Everett[1], Chandan Kumar Gautam[1], David Jackson[2], Lena Maria Müller[1,3#]

*equal contribution

[#]corresponding author

[1]Department of Biology, University of Miami, Coral Gables, FL, USA

[2]Cold Spring Harbor Laboratory, Cold Spring Harbor, NY, USA

[3]The Salk Institute for Biological Studies, La Jolla, CA, USA

[4]School of Biological Sciences, University of California San Diego, La Jolla, CA 92093

Present addresses:

E.X.L.: Stowers Institute for Medical Research, Kansas City, MO 64110

P.L.L.: Department of Botany and Plant Pathology, Oregon State University, Corvallis, OR 97331

H.E.: Systems, Synthetic, and Physical Biology, Rice University, Houston, TX 77005

C.K.G.: Department of Microbiological Sciences, North Dakota State University, Fargo, ND 58108

## Abstract

The CLAVATA signaling pathway regulates plant development and plant-environment interactions. CLAVATA signaling consists of mobile, cell-type or environment-specific CLAVATA3/ESR-related (CLE) peptides, which are perceived by a receptor complex consisting of leucine-rich repeat receptor-like kinases such as CLAVATA1 and receptor-like proteins such as CLAVATA2, which often functions with the pseudokinase CORYNE (CRN). CLAVATA signaling has been extensively studied in various plant species for its role in meristem maintenance and in legumes for modulating root interactions with nitrogen-fixing rhizobia. Some signaling proteins

involved in development and nodulation, including CLAVATA1, also regulate plant interactions with mutualistic arbuscular mycorrhizal (AM) fungi. However, our knowledge on AM symbiosis regulation by CLAVATA signaling remains limited and only a handful of genetic regulators have been identified. Here we report that *Medicago truncatula CRN* controls inflorescence meristem branching and negatively regulates root interactions with AM fungi. *MtCRN* functions partially independently of the AM autoregulation signal *MtCLE53*. Transcriptomic data revealed that *crn* roots display signs of perturbed nutrient, symbiosis, and stress signaling, suggesting that *MtCRN* plays various roles in plant development and interactions with the environment.

## Introduction

Cell-cell communication is critical for plant development and cellular responses to internal and external cues. CLAVATA (CLV) signaling, which consists of mobile CLAVATA3/ESR-related (CLE) peptide hormones and CLE receptor complexes, regulates many aspects of plant development and responses to the environment (Bashyal *et al.*, 2023; Lindsay *et al.*, 2023). CLE receptor complexes consist of leucine-rich repeat receptor-like kinases (LRR-RLKs) with an extracellular LRR ligand-binding domain and an intracellular kinase domain (e.g., CLAVATA1, CLV1, or BARELY ANY MERISTEM, BAM1-3), receptor-like proteins (e.g., CLAVATA2, CLV2) containing an extracellular ligand-binding domain but lack a kinase domain, and other components such as the pseudokinase CORYNE (CRN) (Hazak and Hardtke, 2016). In Arabidopsis and maize, CLV2 and CRN are considered a CLE perception unit (Bleckmann *et al.*, 2009; Je *et al.*, 2018*a*). CLV2-CRN can form complexes with CLV1 or BAMs, but also function independently as a parallel pathway (Guo *et al.*, 2010; Somssich *et al.*, 2016*b*; Hazak *et al.*, 2017). Similarly, the *Medicago truncatula* ortholog of CLV1 (termed SUNN in this species), MtCLV2 and MtCRN can interact with each other (Crook *et al.*, 2016). While the cellular function of CRN is still elusive, co-expression assays in *Nicotiana benthamiana* leaves suggest that the short extracellular domain of AtCRN is important for stabilizing the CRN-CLV2 complex at the plasma membrane, whereas the intracellular kinase domain is important for transmitting CLE peptide signals (Somssich *et al.*, 2016*a*).

59 Mutations in CLV receptors and ligands disrupt meristem organization, often leading to enlarged
60 vegetative, inflorescence and floral shoot meristems (Lindsay *et al.*, 2023). These meristem
61 defects in turn impact floral organization and fruit development, altering the number of flowers
62 produced in an inflorescence, the number of floral organs produced, or the arrangement and
63 size of the fruit. The impact of a particular CLV mutation on meristem organization depends on
64 the specific gene mutated, the nature of the mutation (allele), and the plant species; this
65 phenomenon is thought to be a result of differences in compensatory mechanisms in meristem
66 maintenance among plant species (Rodriguez-Leal *et al.*, 2019). To date, maize and Arabidopsis
67 are the only plant species in which *crn* mutants have been described. In both species, shoot and
68 inflorescence meristems are enlarged. Arabidopsis *crn* mutants produce more carpels per
69 flower, and some flowers make stamens without anthers (Müller *et al.*, 2008). Depending on the
70 temperature, *crn* floral primordia and flowers are prematurely terminated (Jones *et al.*, 2021).
71 Maize *crn* mutants produce fasciated ears, with a disordered arrangement of kernel rows and
72 larger kernel row number (Je *et al.*, 2018*a*). CLV signaling also plays roles in root development,
73 including maintenance of the root apical meristem and protophloem differentiation (Stahl *et al.*,
74 2013; Araya *et al.*, 2014; Hazak *et al.*, 2017). *AtCRN* is expressed in multiple cell types in the
75 root, including stele, endodermis, and quiescent center cells of the meristem (Somssich *et al.*,
76 2016*a*; Hazak *et al.*, 2017). Phloem-expressed AtCRN was shown to be required for the
77 perception of root-active CLE peptides (Hazak *et al.*, 2017). Despite its importance for CLE
78 signaling not all Arabidopsis *crn* mutant alleles show a phenotype characterized by longer
79 primary roots (Müller *et al.*, 2008; Somssich *et al.*, 2016*a*; Hazak *et al.*, 2017), suggesting *CRN* by
80 itself is not required for root development.
81
82 In addition to plant development, CLAVATA signaling pathways also modulate plant interactions
83 with the environment, which includes responses to abiotic and biotic factors such as host
84 responses to pathogenic or beneficial microbes (Bashyal *et al.*, 2023). Mutualistic plant
85 interactions with rhizobia during nodulation or *Glomeromycotina* fungi during arbuscular
86 mycorrhiza (AM) symbiosis are regulated by various receptor-ligand signaling pathways (Roy and
87 Müller, 2022), including CLV signaling. In both symbioses, the host plant provides microbial

88 symbionts with photosynthetically fixed carbon in exchange for mineral nutrients. While
89 rhizobia supply the host with nitrogen (N), AM fungi provide a range of benefits including N,
90 phosphorus (P), and water (Smith and Reid, 2008). Both symbioses are governed by negative
91 regulatory pathways based on plant nutrient (N or P) status and prior microbial colonization
92 (autoregulation); these pathways are mediated by nutrient- or symbiosis-induced CLE peptides,
93 respectively (Roy and Müller, 2022). Autoregulation of nodulation (AON) is a systemic negative
94 feedback loop that has been studied in numerous legume species (Wang *et al.*, 2018). In *M.*
95 *truncatula*, AON is regulated by root-derived, nodule-induced CLE peptides (MtCLE12,
96 MtCLE13), which negatively regulate nodule number in a SUNN- and MtCRN-dependent manner
97 (Schnabel *et al.*, 2005; Crook *et al.*, 2016; Nowak *et al.*, 2019). Grafting experiments revealed
98 that SUNN and MtCRN act in the shoot (Schnabel *et al.*, 2005; Crook *et al.*, 2016); however, both
99 genes are also expressed in roots (Schnabel *et al.*, 2012; Crook *et al.*, 2016), suggesting various
100 functions across tissues and organs. Autoregulation of mycorrhizal symbiosis (AOM) is regulated
101 by the CLE peptide MtCLE53, which is induced in the vascular tissue of colonized roots and
102 negatively regulates AM fungal colonization by repressing biosynthesis of strigolactones (Müller
103 *et al.*, 2019; Karlo *et al.*, 2020). Strigolactones are produced by host plants in response to P and
104 N starvation and promote AM symbiosis (Yoneyama *et al.*, 2007; Gomez-Roldan *et al.*, 2008; Liu
105 *et al.*, 2011; Foo *et al.*, 2013; Marro *et al.*, 2022). In the current AOM model, AM-induced
106 *MtCLE53* down-regulates strigolactone biosynthesis and consequently reduces subsequent AM
107 fungal root colonization (Müller *et al.*, 2019).
108
109 Like AON, AOM depends on CLV1, which has been shown to regulate AM fungal root
110 colonization not only in legumes (e.g., *M. truncatula SUNN*), but also in non-legumes including
111 tomato and the monocot *Brachypodium distachyon*, suggesting conservation of the pathway
112 across plant clades (Wang *et al.*, 2018, 2021; Müller *et al.*, 2019; Wulf *et al.*, 2024). Plants
113 defective in *SUNN* display a hypermycorrhizal phenotype with elevated root colonization levels
114 and arbuscule numbers and are insensitive to *MtCLE53* overexpression (Morandi *et al.*, 2000;
115 Müller *et al.*, 2019; Karlo *et al.*, 2020). Although AON and AOM signal through the same LRR-RLK
116 SUNN, the upstream-acting CLE peptides and downstream signaling appear to at least partially

117 differ between the two symbioses (Mortier *et al.*, 2010; Müller *et al.*, 2019; Karlo *et al.*, 2020;
118 Chaulagain *et al.*, 2023*b*,*a*). Recent evidence from tomato (*Solanum lycopersicum*) suggests that
119 AM symbiosis is regulated by multiple, at least partially independent CLV signaling pathways:
120 grafting experiments revealed that while SlFAB (ortholog of CLV1) acts in the root, SlCLV2 is part
121 of two distinct signaling pathways controlling AM symbiosis from the shoot and the root,
122 respectively (Wang *et al.*, 2021). In addition, the AM-induced SlCLE11 peptide acts as a negative
123 regulator of AM symbiosis but functions independently of SlFAB or SlCLV2 (Wulf *et al.*, 2024). By
124 contrast, hypernodulating pea mutants in *CLV2* (*sym28*), did not show a hypermycorrhizal
125 phenotype, suggesting species-specific differences in symbiosis regulation (Morandi *et al.*,
126 2000). In addition, in contrast to *MtCLE53* over-expression, *sunn* itself (as well as mutants in the
127 tomato and pea orthologs) does not exhibit mis-regulated strigolactone biosynthesis (Foo *et al.*,
128 2014; Müller *et al.*, 2019; Karlo *et al.*, 2020; Wang *et al.*, 2021), suggesting additional signaling
129 components must be involved in MtCLE53-SUNN-mediated AOM signaling that impact
130 strigolactone biosynthesis.
131
132 In addition to autoregulation, AM symbiosis is also tightly regulated by the availability of soil
133 mineral nutrients to the plant. High N or P concentrations in the substrate can suppress AM
134 symbiosis development (Abbott *et al.*, 1984). Although P is the predominant element plants
135 acquire through AM fungi, N starvation can promote AM symbiosis even under high P (Nouri *et*
136 *al.*, 2014). In *M. truncatula*, P-induced *MtCLE33* acts as a negative regulator of AM symbiosis via
137 a SUNN-dependent pathway although SUNN itself is not required for P repression of AM
138 symbiosis (Müller *et al.*, 2019). Similarly, work in tomato revealed that regulation of AM by CLV
139 receptors is independent of plant P but dependent on plant N status (Wang *et al.*, 2021).
140 Despite substantial progress in recent years, our knowledge on AM symbiosis regulation by CLV
141 signaling is incomplete and fragmented across plant species. Like with meristem development,
142 CLV signaling may be differently wired across plant species with different nutrient uptake
143 strategies and capacities for symbiotic interactions.
144

145 Here, we report *MtCRN* as a regulator of *M. truncatula* inflorescence branching. In addition, we
146 find that *MtCRN* acts as a negative regulator of AM symbiosis in *M. truncatula*. Our results
147 further suggest that, while *MtCRN* contributes to AOM, it also regulates AM symbiosis via
148 additional pathways. Transcriptomics data suggest that *crn* mutants display broad alterations in
149 response to biotic and abiotic factors, indicating that MtCRN may integrate multiple signaling
150 pathways with distinct outcomes.
151
152 **Results**
153 ***M. truncatula* CLAVATA signaling regulates inflorescence meristem branching and flowering**
154 **time but is dispensable for root development**
155 Mutants in CLV signaling have previously been described to be impaired in meristem
156 maintenance, with mutants often displaying inflorescence or stem fasciation (Clark *et al.*, 1997).
157 Arabidopsis *CRN* specifically has been reported to modulate inflorescence meristem termination
158 and flower outgrowth under stress (Müller *et al.*, 2008; Jones *et al.*, 2021). *CLV1* orthologs in
159 legumes (*M. truncatula*, *Lotus japonicus,* pea, soybean), which regulate symbiosis, show no
160 shoot apical meristem defects (Searle *et al.*, 2003; Schnabel *et al.*, 2005; Mirzaei *et al.*, 2017;
161 Scott *et al.*, 2024). Intriguingly, soybean is the only one of these species that has a second CLV1
162 gene (*GmCLV1A*); *GmCLV1A* does not regulate symbiosis but modulates shoot branching as well
163 as flower number and development, suggesting functional diversification of the two paralogs
164 (Mirzaei *et al.*, 2017). In addition, other symbiosis-regulating CLV signaling components such as
165 *LjCLV2*, *PsCLV2*, and *LjKLAVIER*, as well as the signaling peptide LjCLV3, affect the size of shoot
166 and inflorescence meristems (Oka-Kira *et al.*, 2005; Miyazawa *et al.*, 2010; Krusell *et al.*, 2011;
167 Okamoto *et al.*, 2011; Scott *et al.*, 2024). Together, this suggests that in legumes, CLV-mediated
168 symbiosis and developmental signaling pathways appear to operate at least partially
169 independently.
170
171 To further dissect CLV signaling during legume development, we investigated above-ground
172 developmental phenotypes of *M. truncatula* mutants carrying a homozygous Tnt1 insertion
173 within the coding sequence of the pseudokinase *MtCRN* (Crook *et al.*, 2016). Time to flowering

174 appeared to be delayed in *crn* when compared to R108 wildtypes (Supplementary Fig.1). Stem
175 fasciation, which is characteristic for many CLV pathway mutants in other species (Somssich *et*
176 *al.*, 2016*b*), was not observed. *M. truncatula* typically produces one solitary flower per
177 inflorescence unit (Fig. 1A, B) (Benlloch *et al.*, 2003). However, we noted that *crn* mutants
178 displayed two flowers per peduncle with high frequency: 91% of 8-week old *crn* (n= 11
179 inflorescences from 3 independent plants) produced two flowers (often with an additional third
180 bud appearing from the same inflorescence, Fig. 1C, D, Supplementary Fig. 1), whereas R108
181 wildtype plants of the same age and grown under the same growth conditions only produced a
182 single flower per peduncle (n=14 inflorescences from 3 independent plants, Fig. 1A, B,
183 Supplementary Fig. 1). Notably, similar inflorescence phenotypes (76% of inflorescences, n=25)
184 were detected in *M. truncatula* mutants defective in the *CLV1* ortholog *SUNN* (*sunn-5*;
185 Supplementary Fig. 1), suggesting both *SUNN* and *MtCRN* modulate inflorescence meristem
186 branching. Although *crn* mutants produced two flowers per peduncle, ultimately only a single
187 seed was produced per inflorescence as one of the two flowers typically appeared to terminate
188 prematurely. In Arabidopsis, *crn* mutants show increased numbers of floral organs and
189 increased inflorescence meristem size (Müller *et al.*, 2008). However, manual dissection of
190 flowers as well as scanning electron microscopy analysis of inflorescences revealed that floral
191 organ numbers and inflorescence width of *M. truncatula crn* did not differ from those in R108
192 wildtypes (Fig. 1 A-G). This indicates that, unlike Arabidopsis and maize, *M. truncatula crn* alters
193 meristem branching, resulting in increased flower number, rather than stem cell proliferation.
194
195 In roots, CLV signaling is critical for root meristem maintenance, lateral root emergence, and
196 protophloem differentiation (Hazak and Hardtke, 2016). We set out to investigate if *M.*
197 *truncatula crn* mutants play a role in root development by analyzing root system architecture of
198 12-day old *crn* and R108 seedlings grown on agar plates. *M. truncatula crn* mutants did not
199 display strong defects in root system development in our experimental growth conditions. We
200 did not detect differences in primary root length, lateral root number, lateral root length, or
201 lateral root density (lateral roots per cm primary root length) between *crn* and R108 seedlings
202 (Supplementary Fig. 2). Similarly, no differences in root length and fresh weight between 4-

203 week-old *crn* and R108 were observed (Supplementary Fig. 2). This is reminiscent of
204 Arabidopsis, where *crn* mutants do not show altered root development although *CRN* is
205 required for the perception of root-active CLE peptides (Müller *et al.*, 2008; Hazak *et al.*, 2017).
206
207 ***MtCRN* negatively regulates AM symbiosis**
208 *M. truncatula* CRN was previously described as a negative regulator of nodulation symbiosis in
209 concert with SUNN (Crook *et al.*, 2016; Nowak *et al.*, 2019). AON, AOM, and nutrient regulation
210 of AM symbiosis share multiple common components, including SUNN, but the role of CRN in
211 AM symbiosis regulation has not been investigated. Because tomato *clv2* mutants are
212 hypermycorrhizal (Wang *et al.*, 2018), CRN-CLV2 are commonly considered a signaling unit
213 (Müller *et al.*, 2008), and MtCRN can interact with the AOM regulator SUNN as well as MtCLV2
214 (Crook *et al.*, 2016), we hypothesized that *MtCRN* may also regulate root interactions with AM
215 fungi. Indeed, *crn* mutants displayed significantly increased overall *Rhizophagus irregularis* root
216 colonization levels relative to the R108 wildtype (Fig. 2A). A detailed analysis revealed that *crn*
217 mutants also show higher arbuscule density (i.e., number of arbuscules per mm colonized root
218 in a defined region at the hyphopodium; see methods) than wildtype roots, whereas vesicle
219 density (vesicles/mm colonized roots) did not differ between the wild-type and the mutant (Fig.
220 2B-E). Intriguingly, similar phenotypes were observed in *Zea mays* (maize) *crn* mutants (Je *et al.*,
221 2018*b*), which showed a slight increase in overall root colonization and significantly higher
222 arbuscule density than B73 wildtype controls (Supplementary Fig. 3). Together, these results are
223 consistent with the hypothesis that *CRN* acts as a negative regulator of AM symbiosis and that
224 this role is conserved across plant clades.
225
226 ***MtCRN* is expressed in colonized and non-colonized roots**
227 To gain further insight into the mechanisms of *MtCRN* regulation of AM symbiosis, we tested
228 the spatial expression pattern of the gene in roots. To do this, we cloned a promoter-reporter
229 construct (*pMtCRN::GUS*) using ~1.9 bp sequence upstream of the *MtCRN* transcription start
230 site and transformed it into A17 wild-type roots using hairy root transformation (Boisson-
231 Dernier *et al.*, 2001). In mock-inoculated roots, we observed strong GUS staining in the

232 vasculature and root tips, including lateral root primordia, as previously observed (Crook *et al.*,
233 2016) (Supplementary Fig. 3). In roots colonized by the AM fungus *R. irregularis*, GUS activity
234 was also observed in colonized cortex cells and adjacent, non-colonized cortex cells, in addition
235 to expression in the vasculature and root tip (Fig. 3A, Supplementary Fig. 3). Although our
236 experiment only allowed us to test spatial expression patterns in roots, transcriptomic data
237 suggest that *MtCRN* is also highly expressed in above-ground tissues (Karlo *et al.*, 2020; Cope *et*
238 *al.*, 2022). Together, this expression pattern suggests that *MtCRN* plays roles in multiple cell
239 types and tissues. In the context of AM symbiosis, the vascular and cortical promoter activity
240 suggests that *MtCRN* may be involved in the perception of local and systemic CLE signals.
241
242 ***MtCRN* functions partially independent of the AOM signal MtCLE53**
243 We previously reported that *MtCRN* is required for *MtCLE16* and *RiCLE1* signaling, plant and
244 fungal *CLE* genes induced in cortex cells upon colonization by AM fungi, respectively (Bashyal *et*
245 *al.*, 2025). The *pMtCRN::GUS* signal detected in colonized cortex regions suggests that cortical
246 MtCRN may be involved in a local response to these CLE peptides. However, our GUS data also
247 suggest high *MtCRN* expression in the vascular tissue, which is indicative of additional roles in
248 other, vascular or systemic CLE signaling pathways. Autoregulation of nodulation (AON) and
249 mycorrhizal symbiosis (AOM) negatively regulates nodulation and AM symbiosis, respectively,
250 based on existing symbioses (Wang *et al.*, 2018). We previously reported that ectopic over-
251 expression of the *M. truncatula* AOM signal *MtCLE53,* which is expressed in the vascular tissue,
252 reduced overall root length colonization in a SUNN-dependent manner (Müller *et al.*, 2019).
253 *MtCRN* has also been implicated in the systemically-acting AON and functions downstream of
254 the nodulation-induced CLE peptides MtCLE12 and MtCLE13 (Nowak *et al.*, 2019). To test if
255 *MtCRN* also acts down-stream of AOM signals, we over-expressed *MtCLE53* under the control of
256 the constitutively active Cauliflower mosaic virus 35S promoter (*35S::MtCLE53*) as well as a
257 control construct (*35S::GUS*) in roots of *crn* mutants and R108 wild-type controls
258 (Supplementary Fig. 3). Similar to what was previously reported for the *M. truncatula* A17
259 accession (Müller *et al.*, 2019; Karlo *et al.*, 2020), ectopic over-expression of *MtCLE53* in roots
260 also reduced overall AM fungal root length colonization in R108. Interestingly, unlike *sunn*,

261 which is fully insensitive to *MtCLE53* over-expression suggesting the LRR-RLK acts in the same
262 pathway as the peptide hormone (Müller *et al.*, 2019), ectopic *MtCLE53* overexpression reduced
263 AM fungal root length colonization also in *crn* (Fig. 3B). However, colonization reduction in
264 *35S::MtCLE53* relative to *35S::GUS*-expressing roots is weaker in *crn* (29%) than in the wild-type
265 background (41%). The partial sensitivity of *crn* to *MtCLE53* over-expression suggests that
266 *MtCRN* is involved in *MtCLE53* signaling but that the AM symbiosis phenotype of *crn* is also
267 influenced by additional, *MtCLE53*-independent pathways.
268
269 **Transcriptomic analysis of *M. truncatula crn* mutants reveals global changes in stress**
270 **response, nutrient homeostasis, and environment interactions**
271 To understand the molecular mechanisms causing the elevated AM fungal root colonization
272 levels in *crn* mutants, we sequenced the transcriptomes of 3 *R. irregularis*-colonized and 4
273 mock-inoculated *crn* and R108 wild-type root systems, respectively (Supplementary table 1). As
274 expected, we observed major transcriptomic changes induced by *R. irregularis* colonization in
275 R108 wild-type roots (434 up-regulated and 266 down-regulated genes, here defined as
276 differentially expressed genes with a log2 fold-change >1 or <-1, respectively, and padj<0.05;
277 Supplementary figures 4-6). Comparing *R. irregularis*-colonized *crn* mutant roots with mock-
278 inoculated *crn* roots, we identified 816 up- and 325-downregulated genes (Supplementary
279 figures 4-5,7). In mock-inoculated *crn* roots relative to mock-inoculated wild-type roots, we
280 identified 1506 up- and 647 down-regulated genes (Supplementary figures 4-5, 8). When
281 comparing differentially expressed genes in *R. irregularis*-colonized *crn* roots with *R. irregularis*-
282 colonized wild-type roots, we identified 1061 up- and 594-downregulated genes
283 (Supplementary figures 4-5, 9, Supplementary table 2). Because *crn* roots are more colonized
284 than wild-type roots, these observed transcriptomic differences may be caused by differences in
285 genotype, differences in AM fungal colonization levels, or both. We performed hierarchical
286 clustering analysis of all differentially expressed genes in *R. irregularis*-inoculated *crn* roots
287 relative to *R. irregularis*-inoculated wild-type roots to identify clusters of differentially expressed
288 genes with similar expression patterns and to distinguish differentially expressed genes solely
289 influenced by colonization levels from those regulated by *MtCRN*.

290

291 Differentially expressed genes were grouped into six clusters (Fig. 4A, Supplementary table 2).
292 Clusters 1, 3 and 6 contained genes that are regulated by AM fungal root colonization, and
293 whose general expression pattern changes were similar in *crn* and wild-type roots. However, the
294 degree of up- or down-regulation differs between the genotypes, likely caused by the
295 differential colonization levels in the mutant compared to the wildtype (Fig. 2 A-E).
296
297 Cluster 1 genes are induced by AM symbiosis and are generally more highly expressed in *R.*
298 *irregularis*-colonized *crn* roots relative to colonized wild-type roots (Fig. 4A). GO analysis of the
299 genes in cluster 1 revealed, among others, an enrichment of genes associated with GO terms
300 related to symbiosis ("AM association", "response to symbiotic fungus", "nodulation"), nitrate
301 assimilation, as well as genes associated with the biosynthesis and transport of secondary
302 metabolites and hormones known to regulate AM symbiosis (e.g., carotenoids, gibberellic acid,
303 brassinosteroids; Fig. 4B, Supplementary table 3). This cluster contains well-studied AM marker
304 genes including but not limited to *MtPT4*, *MtRAM1*, *MtRAM2,* or *MtSTR*, which function in
305 bidirectional nutrient exchange between the symbiotic partner and whose expression is known
306 to be correlated with AM colonization levels (Serrano *et al.*, 2024).
307
308 Clusters 3 and 6 contain genes that are down-regulated by AM fungal root colonization; AM-
309 mediated down-regulation is more pronounced in *crn* roots than in wildtypes. While no
310 significant GO terms were found in cluster 3 (11 genes), in cluster 6 we detected enrichment of
311 GO terms related to cell wall biogenesis and remodeling (Fig. 4D, Supplementary table 3) as well
312 as ethylene signaling. Notably, this GO term contained five transcription factors of the
313 APETALA2/ETHYLENE RESPONSE FACTOR (AP2/ERF) family; however, AP2/ERF transcription
314 factors have a more role in plant stress signaling, and, apart from ethylene, also often respond
315 to the hormones abscisic acid (ABA), gibberellic acid (GA), brassinosteroids (BR), and cytokinin
316 (Xie *et al.*, 2019). To our knowledge, no symbiosis-related function has been reported for any of
317 the AP2/ERF transcription factors in cluster 6.
318

319 Cluster 2 contains 549 genes that are up-regulated in *crn* roots relative to wild-type roots,
320 regardless of AMF colonization status (Fig. 4A). Many genes in this cluster appear to play roles in
321 plant responses to abiotic and biotic stresses: The GO term with the highest fold-enrichment
322 (61-fold) in this cluster is saponin biosynthetic process (Fig. 4C, Supplementary table 3).
323 Saponins are secondary metabolites with antioxidant activity that play various roles in plant-
324 microbe interactions, including plant defense against pathogens and herbivores (Mugford and
325 Osbourn, 2012; Chen *et al.*, 2014). Soy saponins have been identified in root exudates as
326 modulators of plant interactions with rhizosphere microbes (Tsuno *et al.*, 2018; Fujimatsu *et al.*,
327 2020). In addition, 12 peroxidases associated with the GO terms "hydrogen peroxide catabolic
328 process" and "cellular oxidant detoxification" were enriched in cluster 2. Peroxidases are major
329 regulators of cellular reactive oxygen species (ROS) homeostasis (Passardi *et al.*, 2005). ROS play
330 various roles in plants, including response to pathogens and beneficial microbes, including AM,
331 but also development, signaling, and cell growth (Wojtaszek, 1997; Fester and Hause, 2005;
332 Huang *et al.*, 2019). The GO term "cellular modified amino acid metabolic process" was
333 enriched in cluster 2; this GO term contained (among others) 4 genes annotated as glutathione
334 S-transferases, which also have antioxidant activity and are involved in ROS scavenging and
335 cellular detoxification during stress responses (Gullner *et al.*, 2018). Together, this data suggest
336 that cellular oxidative stress may be attenuated in *crn* through increased ROS scavenging.
337 Conversely, *crn* roots display an enrichment of GO terms associated with lipid metabolism ("lipid
338 biosynthetic process", "fatty acid metabolic process", "monocarboxylic acid biosynthetic
339 process") and oxylipin biosynthesis. The latter contained four genes encoding 9-lipoxigenases
340 (*9-LOX*), and one gene annotated as *ALPHA-DIOXYGENASE 1 (αDOX1)*. 9-oxylipins play a role in
341 cellular signaling, defense, and abiotic stress response (Vicente *et al.*, 2012), and their up-
342 regulation suggests that *crn* mutants may have a heightened response to biotic stress even in
343 the absence of microbes. In line with this hypothesis, the GO term "defense response" was also
344 enriched among the genes in cluster 2 (Fig. 4C); this GO term contained several genes encoding
345 NUCLEOTIDE-BINDING SITE LEUCINE-RICH REPEAT (NBS-LRR) family proteins, which can directly
346 bind to microbial effectors and thus play critical roles in plant immune responses to pathogens

347 (Marone *et al.*, 2013). This suggests that, despite signatures of attenuated oxidative stress,
348 other components of the plant response system to biotic stresses are up-regulated in *crn*.
349
350 Furthermore, we detected an enrichment of genes associated with the GO term
351 "transmembrane transport" among the *crn*-upregulated genes in cluster 2. Interestingly, these
352 included, among others, genes encoding transporters for carbon products such as sugar
353 (*MtESL16.1/MtESL2.4, MtESL3.4, MtESL6.4, MtSTP3.2, MtSTP5.1/MtSTP5.2*), which may
354 indicate that carbon flux is altered in *crn*. In addition, we identified putative transporters for
355 nitrate (*MtNPF2.11, MtNPF5.13, MtNPF5.5, MtNPF5.10*), ammonium
356 (*MtrunA17_Chr4g0007621/ MtrunA17_Chr4g0007611*), phosphate (*MtPT2, MtPT9*), metals
357 (*MtMTP8*), potassium (*MtrunA17_Chr4g0055471*), and zinc (*MtZIP6*) among the genes in cluster
358 2 (Supplementary table 2, Supplementary table 3), suggesting mis-regulation of various nutrient
359 uptake or homeostasis pathways in the mutant (further discussed below).
360
361 Cluster 4 contains genes that are down-regulated in *crn* roots relative to wild-type roots with
362 little impact of symbiosis status (Fig. 4A). In this group of 391 genes, only the GO term 'plant-
363 type secondary cell wall biogenesis' was enriched (Supplementary table 3). Intriguingly, all 13
364 genes associated with this GO term in cluster 4 are annotated as FASCICLIN-LIKE
365 ARABINOGALACTAN PROTEIN (FLA). FLAs are extracellular glycoproteins involved in a plethora
366 of functions, including development, growth, and environmental responses (He *et al.*, 2019),
367 but to our knowledge have not been studied in the context of AM symbiosis or CLAVATA
368 signaling. However, genes encoding arabinogalactan proteins as well as other cell wall-related
369 genes have been shown to be down-regulated also in a *A. thaliana crn* mutant (Pallakies and
370 Simon, 2014). This suggests a conserved role of CRN in cell wall organization, which is critical for
371 its function in growth and development.
372
373 Cluster 5 contains 14 genes that are induced in R108 *R. irregularis*-colonized roots relative to
374 mock-inoculated roots but show the opposite pattern in *crn* background (down-regulated in *R.*

375 *irregularis*-colonized roots relative to mock-inoculated *crn* roots) (Fig. 4A, Supplementary table
376 3). No significantly enriched GO terms were detected in cluster 5.
377
378 **N and P homeostasis signaling is perturbed in *crn* roots**
379 Our cluster analysis suggests an up-regulation of multiple mineral nutrient transporters in *crn*,
380 regardless of root colonization status (see above, Supplementary table 3). This suggests that in
381 *crn* mutants, nutrient starvation or homeostasis signaling pathways may be mis-regulated.
382 Because P and N are major regulators of AM symbiosis and their homeostasis is regulated by
383 CLAVATA signaling pathways in various plant species (Bashyal *et al.*, 2023), we examined genes
384 associated with P and N homeostasis more closely in our dataset. Interestingly, 16 genes
385 putatively associated with N homeostasis were regulated by *MtCRN* regardless of root
386 colonization status, and 11 additional ones were found to be synergistically regulated by *MtCRN*
387 and AM status of the plant (Fig. 5A-B, Supplementary table 4). Similarly, eight genes associated
388 with P homeostasis were mis-regulated in *crn* relative to R108 without additional regulation by
389 root colonization status, and an additional three genes were regulated by *MtCRN* and AM
390 symbiosis (Fig. 5C-D, Supplementary table 4). This data suggest a major perturbance in nutrient
391 homeostasis signaling in *crn* even in the absence of symbiosis. Because nutrient starving plants
392 initiate more interactions with beneficial microbes (Nouri *et al.*, 2014), a mis-regulation of
393 nutrient homeostasis or starvation signaling may promote AM fungal root colonization in *crn*. To
394 test this hypothesis, we grew *R. irregularis*-inoculated R108 and *crn* plants under varying
395 phosphate and nitrogen conditions (Supplementary Fig. 3). Under low nitrogen (0.5 mM) with
396 low or high phosphate (20µM or 2 mM, respectively), the *crn* mutant phenotype was
397 suppressed and no difference in root length colonization was detected between the mutant and
398 the wildtype. Conversely, when grown under a high nitrogen (50 mM) fertilization and low
399 phosphate fertilization regime, *crn* mutants displayed higher root length colonization than
400 wildtype controls. The sensitivity of the *crn* mutant phenotype to nitrogen levels is reminiscent
401 to what has been reported for mutants in the CLV1 and CLV2 orthologs in tomato (Wang *et al.*,
402 2021), and indicates that *MtCRN* may participate in a CLAVATA signaling pathway involved in
403 nitrogen regulation of AM symbiosis.

404

405 **Expression of early symbiosis signaling genes is mis-regulated in *crn***

406 Consistent with an increase in AM fungal root colonization, we observed elevated gene
407 expression of known AM-induced genes in *R. irregularis*-colonized *crn* roots relative to colonized
408 wild-type controls (see above). This was the case for well-studied genes involved in arbuscule
409 accommodation and symbiotic nutrient exchange (e.g., *MtPT4*, *MtRAM2*, *MtSTR*), and arbuscule
410 degeneration (e.g., *MtMYB1*, *MtCP3*, *MtTGL*) (Fig. 6A and B, Supplementary table 5). Expression
411 of these genes did not differ when mock-inoculated *crn* roots were compared to mock-
412 inoculated R108 roots.

413

414 Conversely, the expression of many genes involved in pre-symbiotic signaling was perturbed in
415 mock-inoculated *crn* roots relative to mock-inoculated wildtype roots, suggesting these genes
416 may be direct or indirect targets of *MtCRN* signaling: We found that the expression of genes
417 involved in strigolactone biosynthesis and secretion (*MtD27*, *MtCCD7*, *MtCCD8*, *MtPDR1a*) not
418 only responds to AM fungal root colonization in *crn* and R108, but is also differentially regulated
419 in *crn* mock-inoculated roots relative to mock-inoculated wild-type controls (Fig. 6A and B). In
420 addition, *MtCCD8b* and *MtMAX1a*, orthologs of genes involved in strigolactone biosynthesis in
421 other species, as well as *MtMAX2* and *MtD14*, involved in strigolactone signaling and
422 perception, respond to AM fungal root colonization and are also differentially regulated in
423 mock-inoculated *crn* roots relative to controls. Similar trends were observed for the known
424 transcriptional regulators governing strigolactone biosynthesis *NSP1* and *NSP2*. Because the
425 production of AM-symbiosis promoting strigolactones is regulated by P and N status of the plant
426 (Yoneyama *et al.*, 2007, 2012; Liu *et al.*, 2011; Foo *et al.*, 2013; Marro *et al.*, 2022), an up-
427 regulation of the strigolactone biosynthesis pathway may be a consequence of the apparent
428 mis-regulation of N and P homeostasis signaling in *crn* roots (Fig. 5A-D).

429

430 In addition, the expression of several genes involved in the common symbiosis signaling
431 pathway (CSSP) appear to be directly or indirectly regulated by *MtCRN* (Fig. 6A-B). The CSSP is
432 triggered by cellular perception of N-acetylglucosamine (GlcNAc)-derived

433 (lipo)chitooligosaccharide molecules derived from AM fungi or rhizobia (myc-LCOs/COs or nod-
434 LCOs, respectively), and is required for cellular entry of symbiotic microbes at the onset of
435 symbiotic interactions (Oldroyd, 2013). *DMI2*, which encodes a putative co-receptor perceiving
436 microbial signals, was found to be up-regulated in mock-inoculated *crn* roots when compared to
437 R108. Likewise, *DMI3*, *IPD3*, and *VPY*, which regulate cellular signal transduction and symbiosis
438 initiation in response to microbial LCO perception (MacLean *et al.*, 2017; Lindsay *et al.*, 2022)
439 function downstream of *MtCRN* signaling. In addition, *DMI3* and *VPY* expression was also found
440 to be responsive to AM symbiosis (Fig. 6A). Because the CSSP pathway is not only required for
441 the establishment of AM but also nodulation symbiosis, and because *crn* was reported to have a
442 hypermycorrhizal phenotype (this study) and a hypernodulation phenotype in *M. truncatula*
443 (Crook *et al.*, 2016), we hypothesize that *crn* mutants are primed for symbiotic interactions even
444 in the absence of microbes, potentially due to an up-regulation of the symbiosis
445 accommodation program as a result of perturbations in N and P starvation signaling (Li *et al.*,
446 2022). In line with this hypothesis, we found that some genes encoding lysin motif (LysM) RLKs
447 involved in the recognition of nod- and myc-LCOs (e.g., *MtLYK8* and *NFP*, but not *MtLYK3*) are
448 up-regulated in *crn* roots even in the absence of a microbe (Fig. 6 C-D, supplementary table 1,
449 supplementary table 6) (Limpens *et al.*, 2003; Smit *et al.*, 2007; Zhang *et al.*, 2024). Intriguingly,
450 10 additional LysM RLKs or receptor-like proteins (LYK, LYR, LYM) that can bind LCOs but have no
451 known role in nodulation or symbiosis (Buendia *et al.*, 2018) were also up-regulated in *crn*
452 mutants relative to wildtypes (both in *R. irregularis*- or mock-inoculated treatments), suggesting
453 recognition of diverse microbial patterns may be altered in *crn*.
454
455 ***Rhizophagus irregularis* transcriptionally responds to colonizing *crn* roots**
456 To investigate R. *irregularis* responses to host genotype, we mapped our transcriptome reads to
457 the *R. irregularis* DAOM197198 v2.0 genome (Yildirir *et al.*, 2022). About 1.2-3.8 % of the reads
458 mapped to the fungal genome in colonized R108 and *crn* roots (Supplementary table 1). We
459 found 19 genes to be up-, and 10 genes to be down-regulated in *crn* roots relative to wild-type
460 roots (logFC>1 or <-1, padj<0.05; Fig. 7A, supplementary table 7). Among the functionally
461 annotated genes down-regulated in *R. irregularis* colonizing *crn* roots relative to wild-type roots

462 (logFC<-1, padj<0.05), we identified multiple transcripts putatively involved in cellular signaling,
463 including two protein tyrosine kinases, a C2H2 zinc finger transcription factor, and one SAM-
464 domain containing protein, which mediate protein-protein interactions and have many roles,
465 including cellular signaling (Kim, 2003). This suggests that *R. irregularis* modulates signaling in
466 response to colonizing *crn* roots; however, because AM fungi are functionally not well
467 understood, we cannot predict which signaling pathways may be impacted.
468
469 Among the *R. irregularis* genes significantly up-regulated in *crn* roots relative to wild-type roots
470 (logFC>1, padj<0.05), we identified multiple transcripts that suggest fungal N metabolism might
471 be perturbed in *crn* (Fig. 7A). Differentially regulated genes associated with fungal N metabolism
472 include an argininosuccinate synthase (*ASS*), which is involved in the biosynthesis of arginine, a
473 critical component of N storage in AM fungi (Cruz *et al.*, 2007). In addition, among the
474 significantly up-regulated genes we found a transcript annotated as *NmrA (Nitrogen metabolic*
475 *regulation A)-like protein*, which in other fungi is part of a protein complex that functions in
476 transcriptional regulation of N metabolism based on N availability (Andrianopoulos *et al.*, 1998;
477 Stammers, 2001). Both *ASS* and *NmrA* have been predominantly detected in the extraradical
478 mycelium of AM fungi where N is taken up (Dumas-Gaudot *et al.*, 2004; Tian *et al.*, 2010). Other
479 known genes involved in *R. irregularis* N metabolism tended to be up-regulated in *crn* roots
480 relative to wildtypes (Fig. 7B), although the adjusted p-value did not fall below the stringent
481 significance criteria described above. This included the ammonium transporters *GintAMT1* and
482 *GintAMT3*, but not *GintAMT2*, two glutamine synthetases (*GS1, GS2*) and a N transporter (*NT*)
483 (Fellbaum *et al.*, 2012) (Fig. 7B).
484
485 Interestingly, a plasma membrane $H^+$-transporting ATPase HA1 with suggested roles in fungal P
486 sensing (Xie *et al.*, 2022) was also observed among the *R. irregulari*s genes significantly up-
487 regulated in *crn* roots (Fig. 7A). This observation prompted us to examine other transcripts
488 known to be involved in fungal in P homeostasis and transport (Kikuchi *et al.*, 2014, 2016; Xie *et*
489 *al.*, 2022). Although none of the known P homeostasis or transport genes were differentially
490 regulated in *crn* vs. R108 roots, some genes displayed trends toward increased expression in *crn*

491 relative to R108 (Fig. 7C). This included, among others, the Pi:$H^+$ symporter RiPT thought to be
492 involved in fungal P uptake from the environment (Harrison and van Buuren, 1995; Maldonado-
493 Mendoza *et al.*, 2001) and the Pi stress marker PHO2 (Austin and Mayer, 2020).
494
495 In addition, our *R. irregularis* transcriptome displays signs of increased chitin biosynthesis when
496 colonizing *crn* roots (Fig. 7A, Supplementary table 7). Among the *R. irregularis* genes
497 significantly up-regulated in *crn* relative to R108 roots (logFC>1, padj<0.05), we identified a gene
498 encoding a UDP-N-acetylglucosamine diphosphorylase, which catalyzes the formation of
499 GlcNAc, and a chitin synthase, which catalyzes chitin formation from GlcNAc building blocks (Fig.
500 7A) (Chen *et al.*, 2022). Notably, GlcNAc are also building blocks of LCO and CO molecules
501 critical for pre-symbiotic communication with the host. Myc-LCO and CO production is
502 promoted by host strigolactones (Chaulagain *et al.*, 2023*a*); biosynthesis genes for these
503 phytohormones are induced in *crn* roots relative to wildtypes (Fig. 6), which could be linked to
504 the observed up-regulation of GlcNAc in *R. irregularis*. However, while fungal LCO and CO
505 molecules initiate CSSP signaling in the host upon recognition by plant LysM-type RLKs, they
506 also have a more general function in regulating fungal growth and development (Rush *et al.*,
507 2020). In addition, a member of the SGNH hydrolase/GDSL lipase family was up-regulated.
508 Although the specific function of this gene is unknown, SGNH hydrolases catalyze a variety of
509 carbon-modifying reactions (Anderson *et al.*, 2022), which may be related to fungal growth and
510 development within the host plant.
511
512 Together, our fungal transcriptome dataset suggests that *crn* roots stimulate *R. irregularis* N and
513 P metabolism, growth and development. Notably, it is possible that some of these changes are
514 an indirect consequence of higher fungal colonization levels observed in the mutant; however,
515 the lack of differential regulation of *R. irregularis* housekeeping genes between *crn* and wild-
516 type roots (Supplementary table 8) suggests that the observed gene expression differences are
517 not solely caused by increased fungal biomass in *crn* roots. While more research is required, our
518 data support the hypothesis that *R. irregularis* differentially responds to as-yet-unknown signals
519 derived from *crn* and wild-type roots.

520

521 **Discussion**

522 CLV signaling has been reported to modulate various aspects of plant development and
523 responses to the environment (Bashyal *et al.*, 2023; Lindsay *et al.*, 2023). Here we describe *M.*
524 *truncatula CRN* as a central regulator of meristem branching and root interactions with AM
525 fungi.

526

527 Although legume mutants in the CLV signaling pathway have been well-studied in multiple plant
528 species in the context of symbiosis regulation, an effect on meristem development has only
529 been described in soybean and pea (Krusell *et al.*, 2011; Mirzaei *et al.*, 2017; Scott *et al.*, 2024).
530 Soybean encodes two CLV1 copies, one of which controls symbiosis and the other controls
531 meristem development (Mirzaei *et al.*, 2017). Our work contributes to a better understanding
532 of legume inflorescence meristem patterning by revealing a role for *MtCRN* and *SUNN* in this
533 process. Although the molecular mechanisms remain to be determined, several hints in our
534 data and those of others point toward an intersection of auxin and CLV in *M. truncatula*
535 meristem signaling: Auxin is an important regulator of meristem identity, and *AtCRN* was found
536 to act upstream of auxin to control floral primordia outgrowth in Arabidopsis (Jones et al.,
537 2021). The *M. truncatula* auxin transport mutant *smooth leaf margin1* has pleiotropic
538 developmental effects, including multiple flowers per inflorescence that are reminiscent of the
539 *crn* flower phenotype reported here (Zhou et al, 2011), suggesting that *MtCRN* may control
540 auxin-mediated outgrowth in *M. truncatula* floral development similar to what was found in
541 Arabidopsis (Jones et al., 2021). In addition, previous studies reported that *SUNN* regulates
542 shoot-to-root auxin transport to control N response (Jin *et al.*, 2012) and that auxin signaling,
543 among other hormonal pathways, is mis-regulated in *sunn* (Karlo *et al.*, 2020), further
544 supporting the hypothesis that CLV signaling may act upstream of auxin also in the context of *M.*
545 *truncatula* meristem maintenance. Like in Arabidopsis, legume meristem signaling may be
546 controlled by multiple, functionally redundant pathways and/or buffering. Consequently,
547 phenotypes may only be apparent in certain mutant alleles or growth conditions. Because these
548 buffering mechanisms appear distinct among plant species, this may explain why inflorescence

549 meristem branching is primarily affected in Medicago *crn* mutants, resembling the phenotype in
550 other legumes (Krusell *et al.*, 2011; Mirzaei *et al.*, 2017), but inflorescence meristem size is
551 affected in maize and Arabidopsis *crn* mutants (Rodriguez-Leal et al., 2019, Hazak and Hardtke,
552 2016, Je et al., 2016).
553
554 CLV signaling has been previously described to be critical for autoregulation of AM symbiosis
555 (AOM), but our knowledge on the molecular mechanisms remains limited. We previously
556 characterized the AM-induced, vascular tissue-expressed MtCLE53 peptide as a member of the
557 AOM pathway ((Müller *et al.*, 2019; Karlo *et al.*, 2020). *MtCLE53* requires *SUNN* to regulate AM
558 symbiosis (Crook *et al.*, 2016; Müller *et al.*, 2019; Karlo *et al.*, 2020). Because MtCRN and SUNN
559 can interact and are required to perceive nodulation-associated CLE peptides during AON
560 (Crook *et al.*, 2016; Nowak *et al.*, 2019), we hypothesized that MtCRN may also be required for
561 MtCLE53 signaling together with SUNN. However, the data presented here suggest that the
562 negative effect of *MtCLE53* overexpression on AM symbiosis is only partially dependent on
563 *MtCRN*. One explanation for our observation is that MtCLE53 can signal through MtCRN-SUNN
564 but also parallel, MtCRN-independent pathway(s). Such parallel pathways and compensation
565 mechanisms are common in CLAVATA signaling modules (Pallakies and Simon, 2014; Nimchuk,
566 2017; Je *et al.*, 2018*a*; Rodriguez-Leal *et al.*, 2019; Selby and Jones, 2023). Our data also
567 suggests that additional, *MtCLE53*-independent pathways contribute to the elevated AM fungal
568 root colonization observed in *crn*. One of these additional pathways is likely the one regulated
569 by *MtCLE16*, an AM-induced, cortex-expressed, *M. truncatula* CLE peptide that locally promotes
570 AM symbiosis in concert with *MtCRN* (Bashyal *et al.*, 2025). The *MtCRN* promoter activity, which
571 we detected in colonized cortex cells and the vascular tissue, also supports the hypothesis that
572 the pseudokinase plays a dual role in AM symbiosis control through cortical MtCLE16 and
573 vascular MtCLE53 signaling. Multiple CLV signaling pathways also appear to govern AM
574 symbiosis in tomato (*Solanum lycopersicum*); for example, SlCLV2 was reported to regulate AM
575 symbiosis through two distinct local and systemic signaling pathways (Wang *et al.*, 2021; Wulf *et*
576 *al.*, 2024). Notably, the receptor complexes involved in vascular and cortical CLAVATA signaling
577 have not been resolved for AM symbiosis. It is known that CRN can interact not only with CLV1

578 (SUNN) but also other receptors, including CLV2 (Bleckmann *et al.*, 2009; Crook *et al.*, 2016; Je
579 *et al.*, 2018*b*) and BAM3 (Hazak *et al.*, 2017). Interestingly, *MtBAM2* was recently reported to
580 play a role during nodulation symbiosis (Thomas and Frugoli, 2024). Future research should
581 investigate if the same or related RLKs function during AM symbiosis in concert with MtCRN.
582
583 Our transcriptomics experiment revealed that *M. truncatula crn* mutants display signatures of
584 abiotic stress, most notably nutrient starvation as suggested by a transcriptional up-regulation
585 of N, P and other nutrient transporters. Intriguingly, *R. irregularis* also displays signs of disrupted
586 N and P metabolism as indicated by an up-regulation of *NmrA and ASS*. The proteins encoded
587 by these genes are predicted to function in the extracellular mycelium of AM fungi to mediate N
588 utilization and incorporation into arginine (Andrianopoulos *et al.*, 1998; Cruz *et al.*, 2007;
589 Fellbaum *et al.*, 2012). Arginine plays a key role in N translocation from the extra- to the
590 intraradical mycelium in AM fungi (Cruz *et al.*, 2007; Fellbaum *et al.*, 2012). In addition, *R.*
591 *irregularis HA1* expression was increased when colonizing *crn* roots; *RiHA1* was previously
592 implicated in P signaling and uptake by the extraradical mycelium, where it powers Pi:$H^+$
593 symporters to promote phosphate uptake (Ezawa and Saito, 2018; Xie *et al.*, 2022). Together
594 with our host transcriptomics data, this finding suggests that *crn* roots may represent a greater
595 sink for N and P than wild-types and consequently stimulate N and P uptake in the colonizing *R.*
596 *irregularis* symbiont (Cruz *et al.*, 2007). Further research is required to better understand the
597 impact of host genotype and host CLV signaling on symbiont metabolism.
598
599 In the plant, N and P starvation results in the upregulation of genes involved in the biosynthesis
600 of strigolactones, which in turn act as positive regulators of AM symbiosis (Akiyama *et al.*, 2005;
601 Yoneyama *et al.*, 2007; Gomez-Roldan *et al.*, 2008; Liu *et al.*, 2011; Foo *et al.*, 2013, 2014; Marro
602 *et al.*, 2022). Intriguingly, our data reveal that many of these genes are upregulated in *crn*
603 relative to wildtype controls, which may be a direct consequence of the apparent perturbations
604 in N and P signaling in *crn*. Strigolactone biosynthesis is also the target of AOM, and the
605 elevated expression of strigolactone biosynthesis genes may also be caused by an at least partial
606 disruption of AOM. In either case, upregulation of genes involved in the symbiosis-promoting

607 strigolactones in *crn* can explain the elevated root colonization levels in the mutant. Together,
608 our functional and transcriptomic data suggest that MtCRN may act upstream of strigolactone
609 biosynthesis regulation in response to MtCLE53 as well as N and P signaling. Intriguingly, up-
610 regulation of strigolactone biosynthesis genes have not been observed in CLV1 mutants in *M.*
611 *truncatula* (*sunn*), pea (*nark*) or tomato (*fab*) (Foo *et al.*, 2014; Karlo *et al.*, 2020; Wang *et al.*,
612 2021), suggesting that CRN (but not SUNN/FAB) may modulate cross-talk between N and P
613 homeostasis, MtCLE53-mediated autoregulation, and AM fungal root colonization.
614
615 Apart from genes involved in nutrient homeostasis and strigolactone biosynthesis, our
616 transcriptome analysis also suggests that *crn* roots display an upregulation of genes associated
617 with the CSSP. The CSSP is required for cellular entry of the microbial symbionts and is activated
618 upon perception of diffusible LCO or CO signals derived from AM fungi or rhizobia (Oldroyd,
619 2013). Because *crn* has previously been described as a regulator of nodulation symbiosis, an
620 effect of *crn* on CSSP gene expression may contribute not only to the hypermycorrhizal
621 phenotype described here, but also to the hypernodulation phenotype described previously
622 (Crook *et al.*, 2016). It was reported previously in rice that transcription of certain CSSP genes
623 (including orthologs of *MtVPY, DMI2, DMI3, IPD3*, which we found here to be regulated by *crn*)
624 is regulated by the plant phosphate starvation response (Das *et al.*, 2022). In addition,
625 expression of LysM-type RLKs and LysM receptor proteins as well as plant responses to LCO/CO
626 perception depend on N and P status of the plant and are greatly increased upon nutrient
627 starvation (Li *et al.*, 2022). We therefore hypothesize that the perturbed N and P signaling in *crn*
628 promotes AM symbiosis by increasing the expression of genes involved in early symbiosis
629 signaling (strigolactone biosynthesis genes, CSSP genes, LysM-RLKs), which facilitates
630 colonization by AM fungi upon contact. It has been established that nutrient starvation
631 determines the outcome of plant-microbe interactions by fine-tuning plant immune responses,
632 potentially in order to facilitate symbiotic interactions (Paries and Gutjahr, 2023). Consistent
633 with this model, our dataset suggests attenuated oxidative stress in *crn* relative to wildtypes;
634 oxidative stress is a hallmark of responses to abiotic factors but also plant immunity. However,
635 we also detected up-regulation of plant defense genes, suggesting *crn* displays additional

636 signatures of enhanced response to biotic stress. Intriguingly, CLV signaling – including CRN –
637 has been implicated in plant responses to diverse abiotic and biotic stresses, including beneficial
638 and pathogenic microbes (Bashyal *et al.*, 2023; Torres Ascurra and Müller, 2025). For example,
639 *A. thaliana crn* mutants display increased resistance to *Heterodera schachtii* cyst nematodes as
640 well as certain bacterial and oomycete pathogens (*Ralstonia solanacearum* and
641 *Hyaloperonospora arabidopsidis*, respectively), while being more susceptible to *Botrytis*
642 necrotrophic fungi or *Pseudomonas syringae* bacterial infection (Replogle *et al.*, 2011;
643 Hanemian *et al.*, 2016). Together with our data, this suggests that coordination or crosstalk of
644 multiple combined abiotic and biotic stress responses, rather than overall stress signaling, may
645 be impaired in *crn*.
646
647 In summary, our findings suggest that *MtCRN* plays multiple, likely independent, roles in plant
648 development, nutrient homeostasis, and plant interactions with the environment. Based on
649 data from other plant species, where different combinations of CLV1-type receptors, CLV2, and
650 CRN are responsible for the perception of diverse CLE signals in a context- and cell-type-specific
651 manner (Whitewoods, 2021), we propose that *MtCRN* acts downstream of diverse CLE peptides
652 in the context of meristem development, nutrient homeostasis, and plant-microbe interactions.
653 More research is needed to identify additional context-dependent CLE signals and receptors
654 that provide specificity to the various signaling pathways *MtCRN* is involved in.
655
656 **Materials and methods**
657 **Plant materials and growth conditions**
658 Homozygous *M. truncatula crn* (NF3436) and *sunn-5* (NF2262) mutants, both in R108
659 background, were a gift from Dr. Julia Frugoli (Clemson University, SC, USA) and were previously
660 described (Crook *et al.*, 2016; Nowak *et al.*, 2019; Thomas and Frugoli, 2024). For AM
661 inoculation experiments, seeds were extracted from seed pods and scarified using sandpaper or
662 by incubating the seeds in concentrated sulfuric acid for 7 minutes. Seeds were washed 5 times
663 in autoclaved distilled H2O and surface-sterilized with 10% Bleach for 7 minutes. Seeds were
664 rinsed again 5 times in autoclaved distilled H2O and incubated at 4°C for 48 hours. Imbibed

665 seeds were germinated on germination paper (Anchor paper) for 3-5 days at room temperature
666 before transplanting into substrate. Plants were grown as previously described (Chaulagain *et*
667 *al.*, 2023*a*). In brief, germinated seedlings were transplanted into SC10 cone-tainers (Steuwe
668 and Sons) filled with washed and autoclaved substrate mix consisting of play sand and fine
669 vermiculite (1:1 ratio). For inoculated samples, 250 *Rhizophagus irregularis* DAOM197198
670 spores (Premier Tech, Canada) were placed onto a sand layer 5 cm below the surface of the
671 substrate in each cone-tainer. For mock-inoculated samples, an equal amount of distilled water
672 was added onto the sand layer. Plants were grown in a growth chamber under a 16 hour light
673 (24°C)/8 hour dark (22°C) regime at 40% relative humidity. For standard experiments, all cones
674 were fertilized twice per week with 20 ml half-strength Hoagland's fertilizer supplied with 20µM
675 potassium phosphate and 2.5 mM nitrate (potassium nitrate and calcium nitrate). For nutrient
676 manipulation experiments, plants were watered twice weekly with 10 ml of half-strength
677 Hoagland's solution, which was adjusted as follows: nitrate levels were reduced to 0.5 mM and
678 phosphate levels were either 20µM (low nitrogen/low phosphate) or 2 mM (low nitrogen/high
679 phosphate). For high nitrogen/high phosphate, we added 50mM nitrogen and 2mM phosphate,
680 respectively. Concentrations of all other nutrients remained constant. Unless otherwise noted,
681 all plants were harvested 5-6 weeks after inoculation. To enrich for *R. irregularis* colonization,
682 we sampled 5 cm-long root sections centered around the inoculated region. For the
683 transcriptomics experiment, whole root systems were harvested.
684
685 **Transient root transformation**
686 Transient root transformations of *M. truncatula* R108 and *crn* plants with *35S:GUS* and
687 *35S:MtCLE53* constructs were performed as described previously (Boisson-Dernier *et al.*, 2001;
688 Müller *et al.*, 2019). Chimeric plants were inoculated with *R. irregularis* as described above and
689 harvested 6.5 weeks after planting into cone-tainers.
690
691 **Root system phenotyping**
692 Seeds were extracted from seed pods and sterilized as described above. Seeds were then
693 distributed on the bottom of a glass petri dish using water surface tension (Floss *et al.*, 2013).

694 Glass petri plates were placed upside down in a 28°C incubator and seedlings were allowed to
695 germinate overnight. With this method, we were able to obtain seedlings with straight roots.
696 Seedlings were then transferred to 12x12 cm square petri dishes filled with modified Fahraeus
697 (F) medium supplied with 4 g/L Gelzan CM agar (Sigma-Aldrich) (Floss *et al.*, 2013). Plates were
698 placed at a 45° angle in a growth chamber under a 16 hour light (24°C)/8 hour dark (22°C)
699 regime. The bottom 2/3 of the plates was wrapped in aluminum foil to protect the roots from
700 light. Pictures of seedlings were taken every 3 days for 12 days starting with the day of transfer
701 to agar plates (day 0). Root system parameters (primary root length, lateral root length, lateral
702 root number, lateral root density) were analyzed using the SmartRoot package in Fiji (Lobet *et*
703 *al.*, 2011; Schindelin *et al.*, 2012) for each timepoint.
704
705 **GUS staining**
706 The ~1.9 kb *MtCRN* promoter sequence was amplified with Phusion High-Fidelity DNA
707 Polymerase (Thermo Scientific) from genomic DNA of wildtype A17, using the primers indicated
708 in Supplementary Table 9. The *pMtCRN:GUS* construct was created by assembling the *MtCRN*
709 promoter, ß-Glucuronidase, GUS, and the destination vector pKm34GW-RR (Floss *et al.*, 2017)
710 by Gibson cloning using the NEBuilder HiFi DNA Assembly Master Mix. *M. truncatula* A17 roots
711 were transformed and inoculated with *R. irregularis* as described above and harvested 5 weeks
712 after planting. The GUS staining was performed as described previously (Müller *et al.*, 2019),
713 followed by WGA-Alexafluor488 staining to visualize R. *irregularis* (see below). Stained roots
714 were imaged using a BZ-X800LE microscope (Keyence).
715
716 **AM fungus staining, microscopy, and quantification of AM fungal colonization**
717 WGA-Alexafluor488 staining was performed by incubating the roots in 20% KOH for 3-4 days at
718 65°C. Roots were rinsed 3-5 times with distilled water and incubated in 1xPBS overnight.
719 Cleared and washed roots were stained with 0.2 mg/ml WGA-Alexafluor488 (Invitrogen) in
720 1xPBS for at least 6 hours. Stained roots were visualized using a Leica Thunder Imager or a Leica
721 M205 FA stereomicroscope. Root length colonization was assessed using the grid-line method
722 (McGonigle *et al.*, 1990). Arbuscule and vesicle density was quantified as previously described

723 (Müller *et al.*, 2020; Chaulagain *et al.*, 2023*a*). In brief, a minimum of 5 z-stacks each of
724 randomly selected colonized root sections from at least 3 independent root systems were
725 imaged that encompassed all arbuscules in that area. Roots were positioned so that the
726 hyphopodium was at the center of the image to ensure infections were at a comparable
727 developmental stage. Imaged arbuscules were counted using the Fiji Image Analysis Package
728 (Schindelin *et al.*, 2012), which was also used to accurately measure the imaged root length.
729 Arbuscule density (arbuscules/mm) was calculated by dividing the number of arbuscules by the
730 root length. Confocal images were obtained using a Leica SP5 confocal microscope.
731
732 **RNA extraction, cDNA synthesis, and qPCR**
733 RNA extraction, cDNA synthesis, and quantitative PCR were performed as previously described
734 (Müller *et al.*, 2019). The qPCRs were performed on a BioRad CFX384 Real-time system.
735 *MtCLE53* gene expression was normalized to the housekeeping gene *MtEF1a* (elongation
736 factor). See Supplementary table 9 for primer sequences.
737
738 **Transcriptomics**
739 For each genotype (*crn* and R108), 6-week-old mock- (n=4 per genotype) and *R. irregularis*-
740 colonized root systems (n=3 per genotype) were harvested as described above. WGA-
741 Alexafluor488 staining was performed on a subset of the samples to confirm colonization. RNA
742 was extracted from the remaining samples as previously described (Javot *et al.*, 2011). Library
743 preparation and transcriptome sequencing was performed by Novogene Co, Ltd. Samples were
744 enriched for mRNA using poly(A) capture. Paired-end sequencing (PE150) was performed on the
745 Illumina Novaseq X platform. Sequencing raw data are deposited in the NCBI Sequence Read
746 Archive (SRA) (BioProject PRJNA1140176). Filtered reads were mapped against the *M.*
747 *truncatula* Mt4.0v1 genome (downloaded from Phytozome 13) and *R. irregularis* DAOM
748 RhiirDAOM197198 v2.0 (downloaded from the JGI Mycocosm database) genome using HiSAT2
749 (Tang *et al.*, 2014; Kim *et al.*, 2019; Yildirir *et al.*, 2022). Normalized read counts were used to
750 calculate differential gene expression with DESeq2 (Love *et al.*, 2014). For each pairwise
751 comparison, log2-transformed fold changes were obtained for each mapped gene. Differential

752 gene expression was considered significant if the p-value adjusted for multiple comparisons
753 using Benjamini-Hochberg method (padj) was below 0.05. Heatmaps were constructed using
754 FPKM-normalized read counts; rows were clustered using Pearson correlation, columns using
755 Spearman correlation. To identify gene groups with similar expression patterns across samples,
756 hierarchical clustering was performed on FPKM-normalized read counts averaged for each
757 genotype/treatment. The number of clusters (k=6) was determined using the sum of squared
758 error method. GO term analysis for biological process was performed on
759 https://geneontology.org/; visualization of the obtained GO term enrichment results was
760 performed in R.
761
762 **Scanning electron microscopy**
763 For inflorescence phenotyping, plants were grown in 6-inch azalea pots in soil (Promix) under a
764 16 hour light/8 hour dark regime at 20-22°C and watered with distilled water as needed. Axils
765 from 8-week-old plants were dissected with 30 gauge insulin syringe needles to reveal
766 inflorescence meristems under a stereoscope. Meristems and the surrounding tissue were
767 mounted on stubs using double-sided tape and imaged in a Jeol JCM-7000 benchtop scanning
768 electron microscope (SEM) with the following conditions: high vacuum, 15 kV, high probe
769 current, analysis mode. Meristems from SEM images were categorized based on (Benlloch *et al.*,
770 2003) and measured using Fiji.
771
772 **Statistical analyses**
773 Statistical significance between two experimental groups was assessed using a two-sided
774 Student's t-test. In graphs, statistical significances between two groups are represented as
775 follows: ***$p<0.001$; **$p<0.01$; *$p<0.05$. Statistical significance between multiple experimental
776 groups was calculated with ANOVA, followed by Tukey's HSD test for multiple comparisons.
777 Pairwise comparisons were considered statistically significant if $p<0.05$. Significant differences
778 are denoted with different letters. The % reduction of root length colonization shown in Fig. 3
779 was calculated separately for each genotype by the following formula: ((sample $RLC_{35S:CLE53}$ –
780 average $RLC_{35S:GUS}$)/average $RLC_{35S:GUS}$)*100. The % reduction values for each genotype were

781 then compared to each other using student's t-test. See paragraphs 'transcriptomics' for
782 additional details on the statistics used to analyze RNA sequencing data. Graphs show data from
783 individual experiments. All experiments were repeated at least twice with similar results.
784

785 **Acknowledgements**
786 We thank Julia Frugoli (Clemson University, SC) for kindly gifting us the *crn* and *sunn-5* mutant
787 lines.
788

789 **Author contributions**
790 L.M.M. conceived the project. J.O., E.X.L, M.K., Y.C.T.A., S.B., H.E., C.K.G. and L.M.M. performed
791 all experiments except for the inflorescence meristem analyses, which were performed by P.L.L.
792 L.M.M. and D.J. acquired funding for the project. L.M.M. wrote the manuscript with input from
793 all co-authors.
794

795 **Conflict of interest**
796 None to declare.
797

798 **Funding**
799 This work was partially funded by USDA-NIFA award 2022-67013-42820 to L.M.M., an American
800 Society of Plant Biologists (ASPB) Summer Undergraduate Research Fellowship (SURF) to E.X.L.,
801 and Pioneer Fund and Human Frontiers Science Program (HFSP) (LT0020/2025-L) fellowships to
802 Y.C.T.A. P.L.L. and D.J. were funded by USDA-NIFA award 2020-67013-30909 and NSF-IOS
803 2131631.
804

805 **Data availability**
806 Raw data from the transcriptome sequencing has been deposited on the NCBI SRA database
807 (Bioproject ID: PRJNA1140176).
808
809

## Figures and figure legends

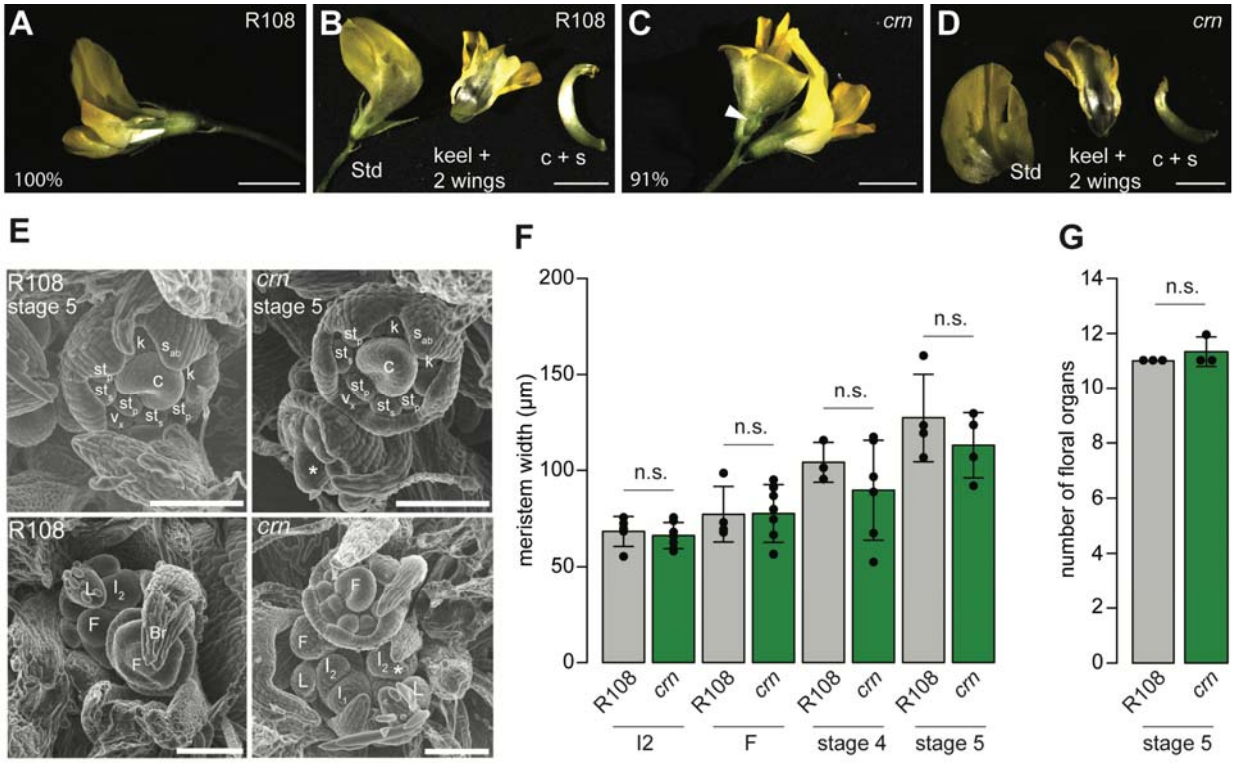


**Figure 1: *M. truncatula CRN* impacts inflorescence development.** A) Close-up of R108 wild-type flower. 100% of inflorescences produced a solitary flower in our growth conditions. B) Dissected wild-type flower. Std, standard petal; fused keel and 2 wing petals; c+s, carpel and stamen. C) Close-up of inflorescence produced by *crn*. Note the additional undeveloped bud (arrowhead). In our growth conditions, 91% of *crn* mutants produced two flowers per inflorescence, the remaining 9% produced solitary flowers similar to the one shown in (A). D) Dissected *crn* flower. Flower organ number and morphology appeared similar to the R108 wildtype shown in (B). (A-D) Scale bars: 0.5 mm. E) Scanning electron microscopy images of R108 and *crn* inflorescence apices. In *M. truncatula*, the primary inflorescence meristem ($I_1$) produces a secondary inflorescence meristem ($I_2$) and leaf primordium (L). The secondary meristem will in turn produce a floral meristem (F), which will differentiate floral organ primordia. Top panels show stage five floral meristems, in which all floral organ primordia have been established. Floral organ primordia size and number are unaltered in *crn*, but there is a second stage 5 floral meristem, indicated with an asterisk. The bottom panel shows a range of floral meristem stages in R108 and *crn*. In *crn,* two $I_2$ meristems are present at the same time, indicated by an asterisk.

827 C, carpel primordium, k, keel petal, $s_{ab}$, abaxial sepal, $st_p$, non-fused vexillary stamen, $st_s$,
828 antesepal stamen, $v_x$, vexillum, Br, bract. Scale bar: 100 µm. F) Width of R108 and *crn*
829 meristems in different floral meristem stages. No effect of the *crn* mutation was observed on
830 meristem width in any developmental stage assessed. $I_2$, secondary inflorescence meristem, F,
831 floral meristem, in which sepal primordia begin to form, stage 4, in which common primordia
832 that will form stamens and petals are formed, stage 5, in which all floral organ primordia have
833 been established. G) Number of stamen and petal floral organ primordia in stage 5 meristems.
834 N.s., no significant difference between R108 and *crn* (Student's t-test).
835
836
837
838
839
840
841
842
843
844
845
846

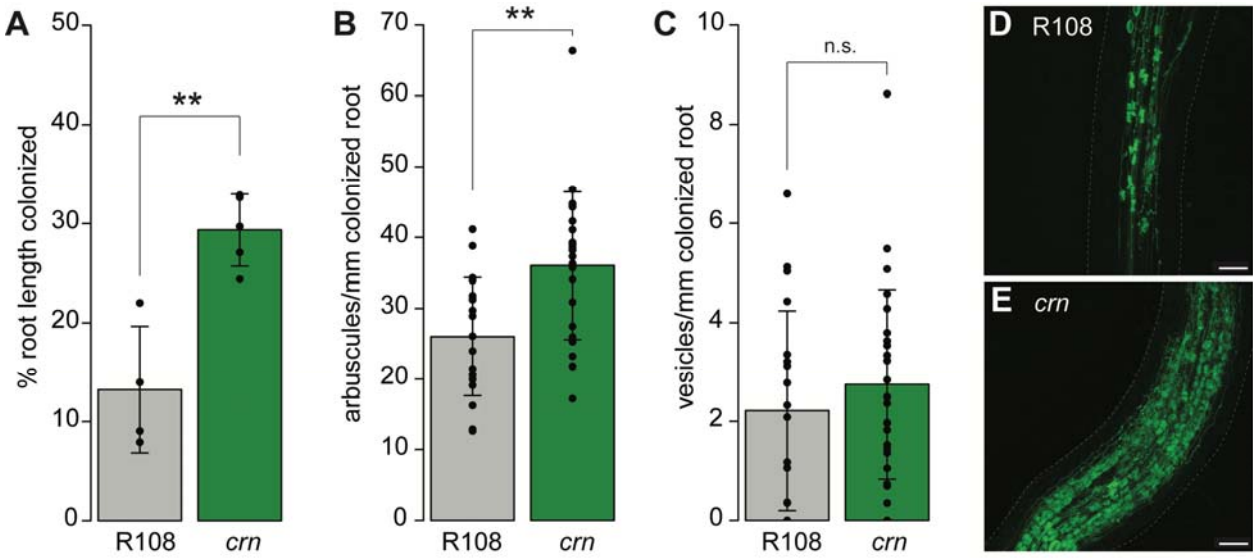


**Figure 2: *M. truncatula crn* mutants display elevated levels of colonization by the AM fungus *R. irregularis*.** A) *crn* mutants display higher levels of overall root length colonization relative to R108 wild-type controls. B) *crn* mutants show higher arbuscule density (number of arbuscules per mm colonized root length) relative to R108 wild-type controls. C) Vesicle density (vesicles per mm colonized root length) does not differ between R108 and *crn*. D) Representative image of an *R. irregularis*-colonized R108 wildtype root. *R. irregularis* was stained with WGA-Alexafluor488 (green). Dashed line: outline of the root. E) Representative image of an *R. irregularis* (green) colonized root section in *crn*. Dashed line: outline of the root. A-C) Bar plots show averages, error bars the standard deviation, points represent individual measurements (i.e., n=4 individual root systems per genotype in A) and n=19 (R108) and n=25 (*crn*) imaged root sections in B) and C), derived from the same root systems as shown in A). Graphs display data from one experiment; this experiment was repeated twice with similar results. ** $p<0.01$ (t-test). Scale bar in D), E): 100 µm.

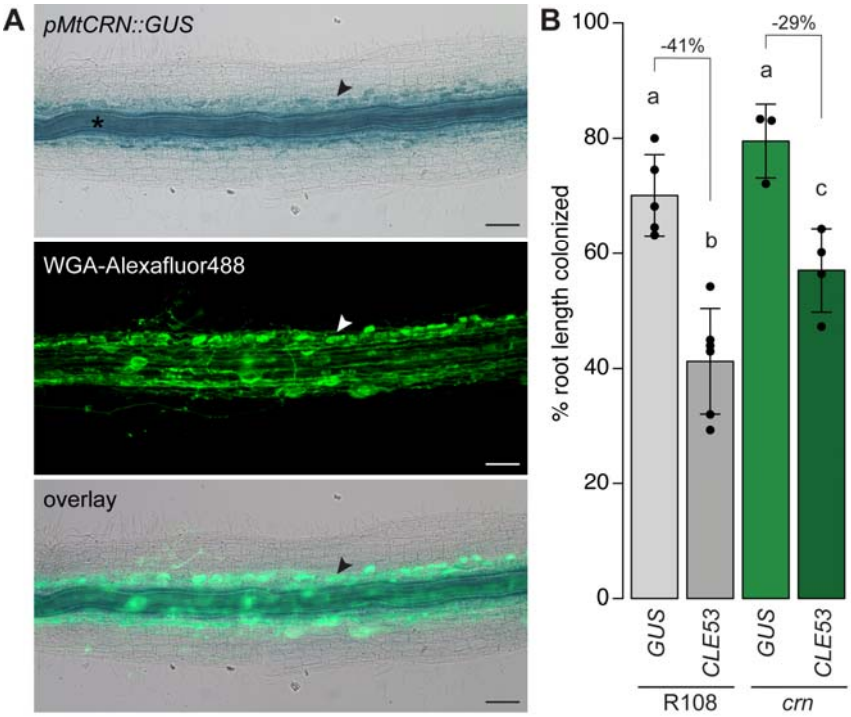


**Figure 3: Expression pattern of *MtCRN* in roots and connection to AOM pathway**. A) Spatial expression pattern of *pMtCRN::GUS* in *R. irregularis*-colonized roots (top); WGA-Alexafluor488 counterstain to visualize *R. irregularis* (middle); overlay of GUS and WGA-Alexafluor488 images (bottom). GUS activity is observed in the vascular tissue (asterisk) and in colonized cortex cells containing arbuscules (arrowhead). Scale bars: 100 µm. B) AM fungal root length colonization of *crn* mutants partially depend on *MtCLE53*. Graph depicts average root length colonization (%) of R108 and *crn* plants transformed with the *35S::GUS (GUS)* or the *35S::MtCLE53 (CLE53)* construct (compare Supplementary Fig. 3C). *MtCLE53* over-expression reduces *R. irregularis* root colonization in R108 and *crn*; however, this suppressive effect is stronger in R108 than in *crn*. For each genotype, the % of colonization reduction upon *MtCLE53* over-expression is shown. The bar graph shows average values; error bars denote standard deviation. Black dots indicate individual datapoints (biological replicates; n=3-5 replicates per sample). This graph displays data from one experiment; the experiment was repeated twice with similar results. Different letters denote significant differences ($p<0.05$) after ANOVA ($p=2.12*10^{-5}$) followed by Tukey's HSD test for pairwise comparisons.

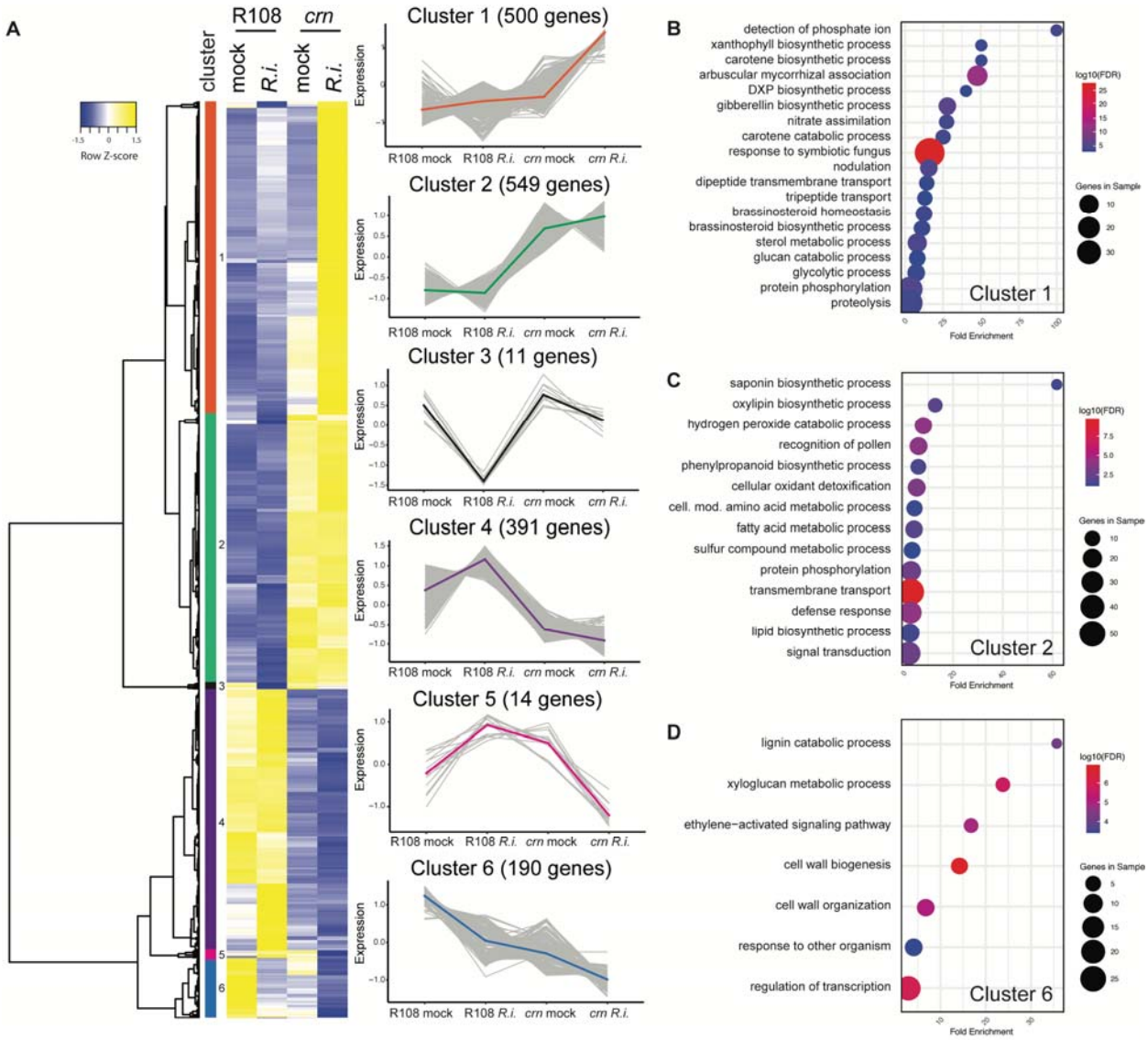


**Figure 4: Hierarchical cluster analysis of differentially expressed genes in *R. irregularis*-colonized and mock-inoculated *crn* and R108 wild-type roots.** A) 1655 genes that are differentially expressed between *R. irregularis*-colonized *crn* and R108 wild-type roots (log2 fold-change >1 or <-1, padj<0.05) were selected for cluster analysis to identify gene groups with similar expression patterns. Genes were clustered using Pearson correlation. Heatmap shows averages of n=4 root samples each for *crn* and R108 mock-inoculated, and n=3 samples each for *crn* and R108 *R. irregularis*-inoculated (*R.i.*). Gene lists for each cluster can be found in table S2. Line graphs display normalized relative expression changes across samples for each individual gene in a cluster (grey) and average changes in color. B) Biological functions GO terms enriched in cluster 1, C) Biological functions GO terms enriched in cluster 2, D) Biological functions GO

890 terms enriched in cluster 6. Note: Cluster 4 has one significantly enriched GO term “plant-type
891 secondary cell wall biogenesis”, which is not shown in this figure. Supplementary tables 2 and 3
892 contain a list of genes for each cluster and the associated GO terms, respectively. DXP, 1-deoxy-
893 d-xylulose 5-phosphate. FDR, false discovery rate.
894
895
896
897
898
899
900
901
902
903
904
905
906
907
908
909
910
911
912
913
914
915
916
917
918

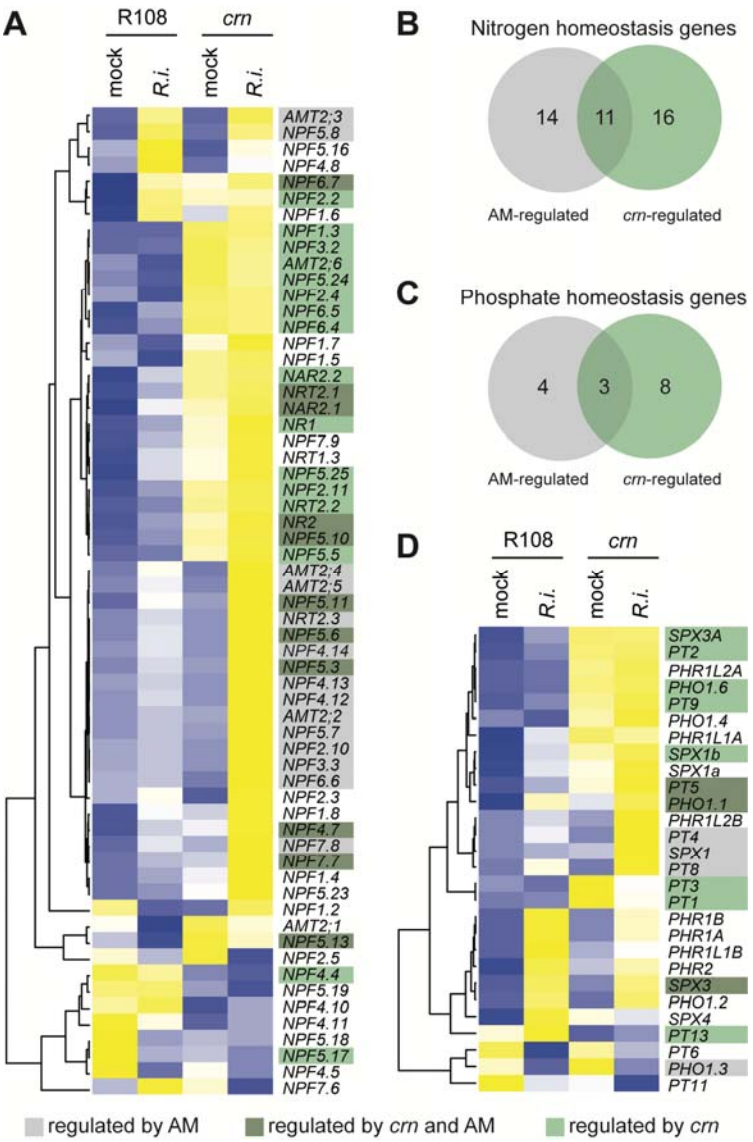


**Figure 5: Differential regulation of N and P homeostasis genes in *crn* mutants.** A) Heatmap for genes annotated as *NITRATE TRANSPORTER (NRT), NITRATE AND PEPTIDE TRANSPORTER FAMILY (NPF), NITRATE ASSIMILATION RELATED (NAR), AMMONIUM TRANSPORTER (AMT),* and *NITRATE REDUCTASE (NR)* with putative roles in *M. truncatula* N metabolism. B) Venn diagram showing the number of putative N homeostasis genes responding to AM symbiosis, *crn*, or both (padj<0.05). C) Venn diagram showing the number of putative P homeostasis genes responding to AM symbiosis, *crn*, or both (padj<0.05). D) Heatmap for genes annotated as *PHOSPHATE TRANSPORTER (PT), PHOSPHATE1 (PHO), PHOSPHATE STARVATION RESPONSE (PHR* and *PHR-LIKE, PHRL),* or *SYG1/PHO81/XPR1 family (SPX)* with putative roles in P homeostasis and transport. A and D) Heatmaps show averages of n=4 root samples each for *crn* and R108 mock-

930 inoculated, and n=3 samples each for *crn* and R108 *R. irregularis*-inoculated (*R.i.*). AM-regulated
931 genes are highlighted in grey, genes differentially regulated in *crn* vs. R108 with no effect of
932 colonization status in light green. Genes responsive to AM and *crn* are highlighted in dark green.
933 B and C) 'AM-regulated' is defined as genes with differential regulation (padj<0.05) between
934 *R.irregularis*-colonized and mock-inoculated R108 and/or *crn* roots, respectively. '*crn*-regulated'
935 is defined as genes with differential regulation (padj<0.05) in mock-inoculated *crn* relative to
936 mock-inoculated R108 roots. Transcript data used to produce these heatmaps can be found in
937 Supplementary table 4.
938
939
940
941
942
943
944
945
946
947
948
949
950
951
952
953
954
955
956
957
958

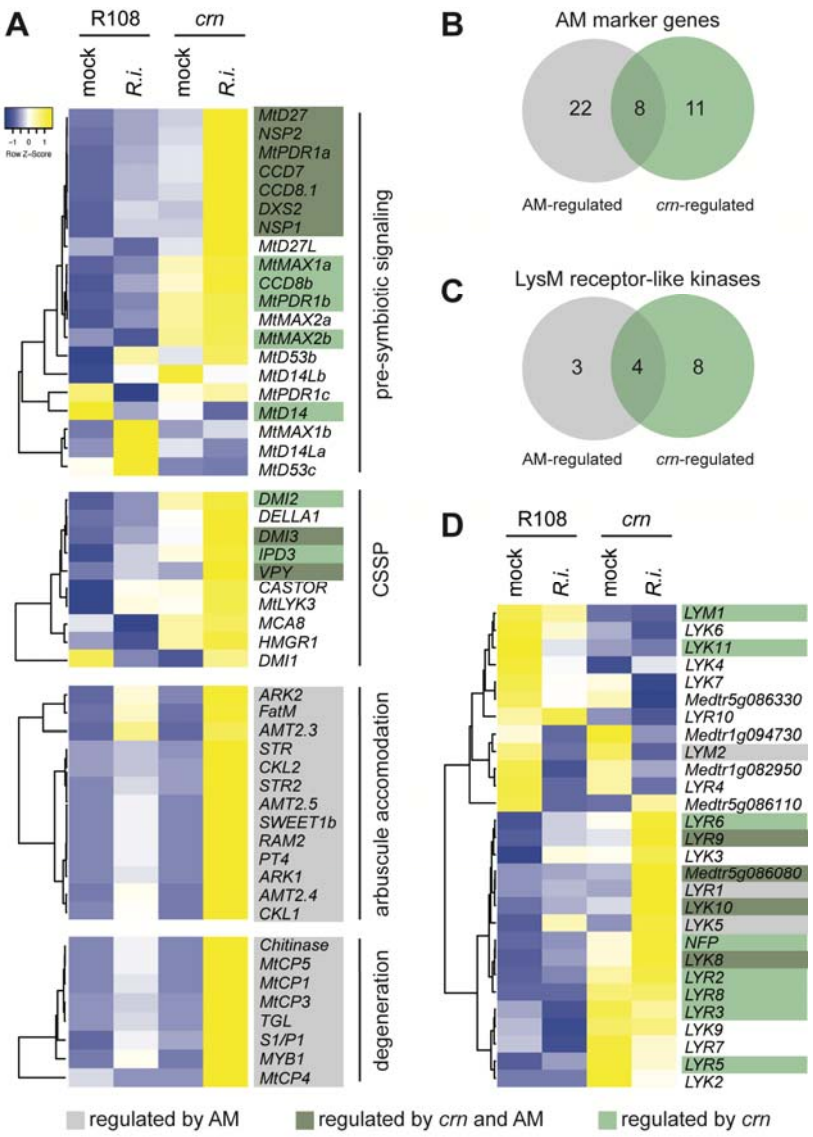


**Figure 6: Differential regulation of AM symbiosis regulators in *crn* mutants.** A) Heatmaps for known genes involved in pre-symbiotic signaling, the common symbiosis signaling pathway (CSSP) shared between AM and nodulation symbiosis, arbuscule accommodation, and arbuscule degradation. B) Venn diagram showing the number of AM regulatory genes from panel A) responding to AM symbiosis, *crn*, or both. C) Venn diagram showing the number of LysM-RLK or LysM receptor protein-encoding genes (LYK, LYR, LYM) responding to AM symbiosis, *crn*, or both. D) Heatmap for LysM-RLK genes in mock- and *R. irregularis*-inoculated wildtype (R108) and *crn* roots. A and D) Heatmaps show averages of n=4 root samples each for *crn* and R108 mock-inoculated, and n=3 samples each for *crn* and R108 *R. irregularis*-inoculated (*R.i.*). AM-regulated

genes are highlighted in grey, genes differentially regulated in *crn* vs. R108 with no effect of colonization status in light green. Genes responsive to AM and *crn* are highlighted in dark green. B and C) 'AM-regulated' is defined as genes with differential regulation (padj<0.05) between *R. irregularis*-colonized and mock-inoculated R108 and/or *crn* roots, respectively. '*crn*-regulated' is defined as genes with differential regulation (padj<0.05) in mock-inoculated *crn* relative to mock-inoculated R108 roots. Transcript data used to produce these heatmaps can be found in supplementary tables 5 and 6.

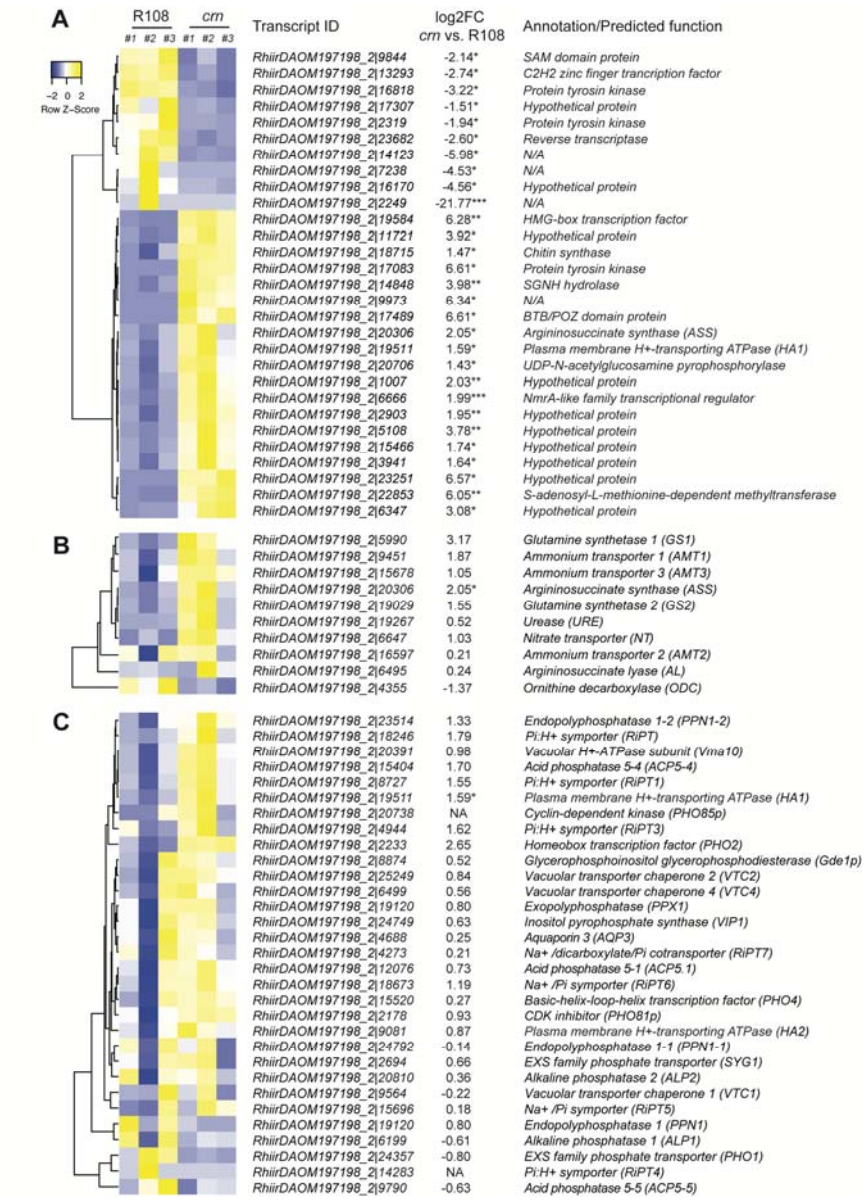


**Figure 7: Host genotype-dependent regulation of *R. irregularis* gene expression.** A) Differentially expressed *R. irregularis* genes (log2 fold change >1 or <-1, padj<0.05) in *crn* and R108 roots. B) Heatmap of genes involved in fungal N metabolism. C) Heatmap of genes involved in fungal P metabolism. Significance: ***adjusted p-value (padj)<0.05, **padj<0.01, *padj<0.05; if no symbol is shown, fungal gene expression does not significantly differ between host genotypes. Transcript data used to produce these heatmaps can be found in supplementary table 7. Data for the same Argininosuccinate synthase (*ASS*) gene are shown in panels A) and B); data for the same $H^+$-transporting ATPase (*HA1*) gene are shown in panels A) and C).

## References


**Abbott LK, Robson AD, de Boer G**. 1984. THE EFFECT OF PHOSPHORUS ON THE FORMATION OF HYPHAE IN SOIL BY THEVESICULAR-ARBUSCULAR MYCORRHIZAL FUNGUS, *GLOMUS FASCICULATUM*. The new phytologist **97**, 437–446.

**Akiyama K, Matsuzaki K-I, Hayashi H**. 2005. Plant sesquiterpenes induce hyphal branching in arbuscular mycorrhizal fungi. Nature **435**, 824–827.

**Anderson AC, Stangherlin S, Pimentel KN, Weadge JT, Clarke AJ**. 2022. The SGNH hydrolase family: a template for carbohydrate diversity. Glycobiology **32**, 826.

**Andrianopoulos A, Kourambas S, Sharp JA, Davis MA, Hynes MJ**. 1998. Characterization of the Aspergillus nidulans nmrA gene involved in nitrogen metabolite repression. Journal of bacteriology **180**, 1973–1977.

**Araya T, Miyamoto M, Wibowo J, Suzuki A, Kojima S, Tsuchiya YN, Sawa S, Fukuda H, von Wirén N, Takahashi H**. 2014. CLE-CLAVATA1 peptide-receptor signaling module regulates the expansion of plant root systems in a nitrogen-dependent manner. Proc Natl Acad Sci **111**, 2029–2034.

**Austin S, Mayer A**. 2020. Phosphate homeostasis – A vital metabolic equilibrium maintained through the INPHORS signaling pathway. Frontiers in microbiology **11**.

**Bashyal S, Everett H, Matsuura S, Müller LM**. 2025. A plant CLE peptide and its fungal mimic promote arbuscular mycorrhizal symbiosis via CRN-mediated ROS suppression. Proceedings of the National Academy of Sciences of the United States of America **122**, e2422215122.

**Bashyal S, Gautam CK, Müller LM**. 2023. CLAVATA signaling in plant–environment interactions. Plant physiology doi: 10.1093/plphys/kiad591.

**Benlloch R, Navarro C, Beltrán J, Cañas LA**. 2003. Floral development of the model legume Medicago truncatula: ontogeny studies as a tool to better characterize homeotic mutations. Sexual plant reproduction **15**, 231–241.

**Bleckmann A, Weidtkamp-Peters S, Seidel CAM, Simon R**. 2009. Stem cell signaling in Arabidopsis requires CRN to localize CLV2 to the plasma membrane. Plant physiology **152**, 166–176.

**Boisson-Dernier A, Chabaud M, Garcia F, Bécard G, Rosenberg C, Barker DG**. 2001. Agrobacterium rhizogenes-transformed roots of Medicago truncatula for the study of nitrogen-fixing and endomycorrhizal symbiotic associations. Molecular plant-microbe interactions: MPMI **14**, 695–700.

**Buendia L, Girardin A, Wang T, Cottret L, Lefebvre B**. 2018. LysM Receptor-Like Kinase and LysM Receptor-Like Protein Families: An Update on Phylogeny and Functional Characterization. Frontiers in plant science **9**, 539.

**Chaulagain D, Schnabel E, Crook A, Bashyal S, Müller LM, Frugoli J**. 2023*a*. A mutation in mediator subunit MED16A suppresses nodulation and increases arbuscule density in Medicago truncatula. Journal of plant growth regulation doi: 10.1007/s00344-023-10993-2.

**Chaulagain D, Schnabel E, Lin EX, Garcia RR, Noorai RE, Müller LM, Frugoli JA**. 2023*b*. *TML1*AND*TML2*SYNERGISTICALLY REGULATE NODULATION BUT NOT ARBUSCULAR MYCORRHIZA IN*MEDICAGO TRUNCATULA*. bioRxiv.

**Chen W, Cao P, Liu Y, *et al.*** 2022. Structural basis for directional chitin biosynthesis. Nature **610**, 402–408.

**Chen Y, Miao Y, Huang L, Li J, Sun H, Zhao Y, Yang J, Zhou W**. 2014. Antioxidant activities of saponins extracted from Radix Trichosanthis: an in vivo and in vitro evaluation. BMC complementary and alternative medicine **14**, 86.

**Clark SE, Williams RW, Meyerowitz EM**. 1997. The CLAVATA1 gene encodes a putative receptor kinase that controls shoot and floral meristem size in Arabidopsis. Cell **89**, 575–585.

**Cope KR, Kafle A, Yakha JK, Pfeffer PE, Strahan GD, Garcia K, Subramanian S, Bücking H**. 2022. Physiological and transcriptomic response of Medicago truncatula to colonization by high- or low-benefit arbuscular mycorrhizal fungi. Mycorrhiza **32**, 281–303.

**Crook AD, Schnabel EL, Frugoli JA**. 2016. The systemic nodule number regulation kinase SUNN in Medicago truncatula interacts with MtCLV2 and MtCRN. The Plant journal: for cell and molecular biology **88**, 108–119.

**Cruz C, Egsgaard H, Trujillo C, Ambus P, Requena N, Martins-Loução MA, Jakobsen I**. 2007. Enzymatic evidence for the key role of arginine in nitrogen translocation by arbuscular mycorrhizal fungi. Plant physiology **144**, 782–792.

**Das D, Paries M, Hobecker K, Gigl M, Dawid C, Lam H-M, Zhang J, Chen M, Gutjahr C**. 2022. PHOSPHATE STARVATION RESPONSE transcription factors enable arbuscular mycorrhiza symbiosis. Nature communications **13**, 1–12.

**Dumas-Gaudot E, Valot B, Bestel-Corre G, Recorbet G, St-Arnaud M, Fontaine B, Dieu M, Raes M, Saravanan RS, Gianinazzi S**. 2004. Proteomics as a way to identify extra-radicular fungal proteins from Glomus intraradicesâ RiT-DNA carrot root mycorrhizas. FEMS microbiology ecology **48**, 401–411.

**Ezawa T, Saito K**. 2018. How do arbuscular mycorrhizal fungi handle phosphate? New insight into fine-tuning of phosphate metabolism. The new phytologist **220**, 1116–1121.

**Fellbaum CR, Gachomo EW, Beesetty Y, Choudhari S, Strahan GD, Pfeffer PE, Kiers ET, Bücking H**. 2012. Carbon availability triggers fungal nitrogen uptake and transport in arbuscular mycorrhizal symbiosis. Proceedings of the National Academy of Sciences of the United States of America **109**, 2666–2671.

**Fester T, Hause G**. 2005. Accumulation of reactive oxygen species in arbuscular mycorrhizal roots. Mycorrhiza **15**, 373–379.

**Floss DS, Gomez SK, Park H-J, MacLean AM, Müller LM, Bhattarai KK, Lévesque-Tremblay V, Maldonado-Mendoza IE, Harrison MJ**. 2017. A Transcriptional Program for Arbuscule Degeneration during AM Symbiosis Is Regulated by MYB1. Current biology: CB **27**, 1206–1212.

**Floss DS, Schmitz AM, Starker CG, Gantt JS, Harrison MJ**. 2013. Gene Silencing in Medicago truncatula Roots Using RNAi. Methods in molecular biology (Clifton, N.J.). Legume Genomics. Totowa, NJ: Humana Press, 163–177.

**Foo E, Ferguson BJ, Reid JB**. 2014. The potential roles of strigolactones and brassinosteroids in the autoregulation of nodulation pathway. Annals of botany **113**, 1037–1045.

**Foo E, Yoneyama K, Hugill CJ, Quittenden LJ, Reid JB**. 2013. Strigolactones and the regulation of pea symbioses in response to nitrate and phosphate deficiency. Molecular plant **6**, 76–87.

**Fujimatsu T, Endo K, Yazaki K, Sugiyama A**. 2020. Secretion dynamics of soyasaponins in soybean roots and effects to modify the bacterial composition. Plant direct **4**.

**Genre A, Chabaud M, Balzergue C, *et al.*** 2013. Short-chain chitin oligomers from arbuscular mycorrhizal fungi trigger nuclear Ca2+ spiking in Medicago truncatula roots and their production is enhanced by strigolactone. The New phytologist **198**, 190–202.

**Gomez-Roldan V, Fermas S, Brewer PB, *et al.*** 2008. Strigolactone inhibition of shoot branching. Nature **455**, 189–194.

**Gullner G, Komives T, Király L, Schröder P**. 2018. Glutathione S-Transferase Enzymes in Plant-Pathogen Interactions. Frontiers in plant science **9**.

**Guo Y, Han L, Hymes M, Denver R, Clark SE**. 2010. CLAVATA2 forms a distinct CLE-binding receptor complex regulating Arabidopsis stem cell specification. The Plant journal: for cell and molecular biology **63**, 889–900.

**Hanemian M, Barlet X, Sorin C, *et al.*** 2016. Arabidopsis CLAVATA1 and CLAVATA2 receptors contribute to Ralstonia solanacearum pathogenicity through a miR169-dependent pathway. The new phytologist **211**, 502–515.

**Harrison MJ, van Buuren ML**. 1995. A phosphate transporter from the mycorrhizal fungus Glomus versiforme. Nature **378**, 626–629.

**Hazak O, Brandt B, Cattaneo P, Santiago J, Rodriguez-Villalon A, Hothorn M, Hardtke CS**. 2017. Perception of root-active CLE peptides requires CORYNE function in the phloem vasculature. EMBO reports **18**, 1367–1381.

**Hazak O, Hardtke CS**. 2016. CLAVATA 1-type receptors in plant development. Journal of experimental botany **67**, 4827–4833.

**He J, Zhao H, Cheng Z, Ke Y, Liu J, Ma H**. 2019. Evolution analysis of the fasciclin-like arabinogalactan proteins in plants shows variable fasciclin-AGP domain constitutions. International journal of molecular sciences **20**, 1945.

**Huang H, Ullah F, Zhou D-X, Yi M, Zhao Y**. 2019. Mechanisms of ROS regulation of plant development and stress responses. Frontiers in plant science **10**.

**Javot H, Penmetsa RV, Breuillin F, Bhattarai KK, Noar RD, Gomez SK, Zhang Q, Cook DR, Harrison MJ**. 2011. Medicago truncatula mtpt4 mutants reveal a role for nitrogen in the regulation of arbuscule degeneration in arbuscular mycorrhizal symbiosis. The Plant journal: for cell and molecular biology **68**, 954–965.

**Je BI, Xu F, Wu Q, Liu L, Meeley R, Gallagher JP, Corcilius L, Payne RJ, Bartlett ME, Jackson D**. 2018*a*. The CLAVATA receptor FASCIATED EAR2 responds to distinct CLE peptides by signaling through two downstream effectors. eLife **7**, e35673.

**Je BI, Xu F, Wu Q, Liu L, Meeley R, Gallagher JP, Corcilius L, Payne RJ, Bartlett ME, Jackson D**. 2018*b*. The CLAVATA receptor FASCIATED EAR2 responds to distinct CLE peptides by signaling through two downstream effectors. eLife **7**.

**Jin J, Watt M, Mathesius U**. 2012. The autoregulation gene SUNN mediates changes in root organ formation in response to nitrogen through alteration of shoot-to-root auxin transport. Plant physiology **159**, 489–500.

**Jones DS, John A, VanDerMolen KR, Nimchuk ZL**. 2021. CLAVATA signaling ensures reproductive development in plants across thermal environments. Current biology: CB **31**, 220-227.e5.

**Karlo M, Boschiero C, Landerslev KG, Blanco GS, Wen J, Mysore KS, Dai X, Zhao PX, de Bang TC**. 2020. The CLE53–SUNN genetic pathway negatively regulates arbuscular mycorrhiza root colonization in Medicago truncatula. Journal of Experimental Botany **71**, 4972–4984.

**Kikuchi Y, Hijikata N, Ohtomo R, Handa Y, Kawaguchi M, Saito K, Masuta C, Ezawa T**. 2016. Aquaporin-mediated long-distance polyphosphate translocation directed towards the host in arbuscular mycorrhizal symbiosis: application of virus-induced gene silencing. The new phytologist **211**, 1202–1208.

**Kikuchi Y, Hijikata N, Yokoyama K, Ohtomo R, Handa Y, Kawaguchi M, Saito K, Ezawa T**. 2014. Polyphosphate accumulation is driven by transcriptome alterations that lead to

near-synchronous and near-equivalent uptake of inorganic cations in an arbuscular mycorrhizal fungus. The new phytologist **204**, 638–649.

**Kim C**. 2003. SAM domains: uniform structure, diversity of function. Trends in biochemical sciences **28**, 625–628.

**Kim D, Paggi JM, Park C, Bennett C, Salzberg SL**. 2019. Graph-based genome alignment and genotyping with HISAT2 and HISAT-genotype. Nature biotechnology **37**, 907–915.

**Krusell L, Sato N, Fukuhara I, *et al.*** 2011. The *Clavata2* genes of pea and *Lotus japonicus* affect autoregulation of nodulation. The Plant journal: for cell and molecular biology **65**, 861–871.

**Li X-R, Sun J, Albinsky D, *et al.*** 2022. Nutrient regulation of lipochitooligosaccharide recognition in plants via NSP1 and NSP2. Nature communications **13**, 6421.

**Limpens E, Franken C, Smit P, Willemse J, Bisseling T, Geurts R**. 2003. LysM Domain Receptor Kinases Regulating Rhizobial Nod Factor-Induced Infection. Science **302**, 630–633.

**Lindsay PL, Ivanov S, Pumplin N, Zhang X, Harrison MJ**. 2022. Distinct ankyrin repeat subdomains control VAPYRIN locations and intracellular accommodation functions during arbuscular mycorrhizal symbiosis. Nature communications **13**, 5228.

**Lindsay P, Swentowsky KW, Jackson D**. 2023. Cultivating potential: Harnessing plant stem cells for agricultural crop improvement. Molecular plant doi: 10.1016/j.molp.2023.12.014.

**Liu W, Kohlen W, Lillo A, *et al.*** 2011. Strigolactone biosynthesis in Medicago truncatula and rice requires the symbiotic GRAS-type transcription factors NSP1 and NSP2. The Plant cell **23**, 3853–3865.

**Lobet G, Pagès L, Draye X**. 2011. A novel image-analysis toolbox enabling quantitative analysis of root system architecture. Plant physiology **157**, 29–39.

**Love MI, Huber W, Anders S**. 2014. Moderated estimation of fold change and dispersion for RNA-seq data with DESeq2. Genome biology **15**, 550.

**MacLean AM, Bravo A, Harrison MJ**. 2017. Plant Signaling and Metabolic Pathways Enabling Arbuscular Mycorrhizal Symbiosis. The Plant cell **29**, 2319–2335.

**Maldonado-Mendoza IE, Dewbre GR, Harrison MJ**. 2001. A phosphate transporter gene from the extra-radical mycelium of an arbuscular mycorrhizal fungus *Glomus intraradices* is regulated in response to phosphate in the environment. Molecular plant-microbe interactions: MPMI **14**, 1140–1148.

**Marone D, Russo M, Laidò G, De Leonardis A, Mastrangelo A**. 2013. Plant nucleotide binding site–leucine-rich repeat (NBS-LRR) genes: Active guardians in host defense responses. International journal of molecular sciences **14**, 7302–7326.

**Marro N, Lidoy J, Chico MÁ, Rial C, García J, Varela RM, Macías FA, Pozo MJ, Janoušková M, López-Ráez JA**. 2022. Strigolactones: New players in the nitrogen–phosphorus signalling interplay. Plant, cell & environment **45**, 512–527.

**McGonigle PT, Miller MH, Evans DG, Fairchild GL, Swan JA**. 1990. A new method which gives an objective measure of colonization of roots by vesicular-arbuscular mycorrhizal fungi. The New phytologist **150**, 495–501.

**Mirzaei S, Batley J, El-Mellouki T, Liu S, Meksem K, Ferguson BJ, Gresshoff PM**. 2017. Neodiversification of homeologous CLAVATA1-like receptor kinase genes in soybean leads to distinct developmental outcomes. Scientific reports **7**.

**Miyazawa H, Oka-Kira E, Sato N, *et al.*** 2010. The receptor-like kinase KLAVIER mediates systemic regulation of nodulation and non-symbiotic shoot development in Lotus japonicus. Development **137**, 4317–4325.

**Morandi D, Sagan M, Prado-Vivant E, Duc G**. 2000. Influence of genes determining supernodulation on root colonization by the mycorrhizal fungus Glomus mosseae in Pisum sativum and Medicago truncatula mutants. Mycorrhiza **10**, 37–42.

**Mortier V, Den Herder G, Whitford R, Van de Velde W, Rombauts S, D'Haeseleer K, Holsters M, Goormachtig S**. 2010. CLE peptides control Medicago truncatula nodulation locally and systemically. Plant physiology **153**, 222–237.

**Mugford ST, Osbourn A**. 2012. Saponin synthesis and function. Isoprenoid Synthesis in Plants and Microorganisms. New York, NY: Springer New York, 405–424.

**Müller R, Bleckmann A, Simon R**. 2008. The receptor kinase CORYNE of Arabidopsis transmits the stem cell-limiting signal CLAVATA3 independently of CLAVATA1. The plant cell **20**, 934–946.

**Müller LM, Campos-Soriano L, Lévesque-Tremblay V, Bravo A, Daniels DA, Pathak S, Park H-J, Harrison MJ**. 2020. Constitutive Overexpression of RAM1 Leads to an Increase in Arbuscule Density in Brachypodium distachyon. Plant physiology **184**, 1263.

**Müller LM, Flokova K, Schnabel E, Sun X, Fei Z, Frugoli J, Bouwmeester HJ, Harrison MJ**. 2019. A CLE–SUNN module regulates strigolactone content and fungal colonization in arbuscular mycorrhiza. Nature plants **5**, 933–939.

**Nimchuk ZL**. 2017. CLAVATA1 controls distinct signaling outputs that buffer shoot stem cell proliferation through a two-step transcriptional compensation loop. PLoS genetics **13**, e1006681.

**Nouri E, Breuillin-Sessoms F, Feller U, Reinhardt D**. 2014. Phosphorus and nitrogen regulate arbuscular mycorrhizal symbiosis in petunia hybrida. PloS one **9**, e90841.

**Nowak S, Schnabel E, Frugoli J**. 2019. The Medicago truncatula CLAVATA3-LIKE CLE12/13 signaling peptides regulate nodule number depending on the CORYNE but not the COMPACT ROOT ARCHITECTURE2 receptor. Plant signaling & behavior **14**, 1598730.

**Oka-Kira E, Tateno K, Miura K-I, *et al.*** 2005. *klavier* (*klv*), A novel hypernodulation mutant of *Lotus japonicus* affected in vascular tissue organization and floral induction. The Plant journal: for cell and molecular biology **44**, 505–515.

**Okamoto S, Nakagawa T, Kawaguchi M**. 2011. Expression and functional analysis of a CLV3-like gene in the model legume Lotus japonicus. Plant & cell physiology **52**, 1211–1221.

**Oldroyd GED**. 2013. Speak, friend, and enter: signalling systems that promote beneficial symbiotic associations in plants. Nature reviews. Microbiology **11**, 252–263.

**Pallakies H, Simon R**. 2014. The CLE40 and CRN/CLV2 signaling pathways antagonistically control root meristem growth in Arabidopsis. Molecular plant **7**, 1619–1636.

**Paries M, Gutjahr C**. 2023. The good, the bad, and the phosphate: regulation of beneficial and detrimental plant–microbe interactions by the plant phosphate status. The new phytologist **239**, 29–46.

**Passardi F, Cosio C, Penel C, Dunand C**. 2005. Peroxidases have more functions than a Swiss army knife. Plant cell reports **24**, 255–265.

**Replogle A, Wang J, Bleckmann A, Hussey RS, Baum TJ, Sawa S, Davis EL, Wang X, Simon R, Mitchum MG**. 2011. Nematode CLE signaling in Arabidopsis requires CLAVATA2 and CORYNE. The Plant journal: for cell and molecular biology **65**, 430–440.

**Rodriguez-Leal D, Xu C, Kwon C-T, *et al.*** 2019. Evolution of buffering in a genetic circuit controlling plant stem cell proliferation. Nature genetics **51**, 786–792.

**Roy S, Müller LM**. 2022. A rulebook for peptide control of legume-microbe endosymbioses. Trends in plant science **27**, 870–889.

**Rush TA, Puech-Pagès V, Bascaules A, *et al.*** 2020. Lipo-chitooligosaccharides as regulatory signals of fungal growth and development. Nature communications **11**.

**Schindelin J, Arganda-Carreras I, Frise E, *et al.*** 2012. Fiji: an open-source platform for biological-image analysis. Nature methods **9**, 676–682.

**Schnabel E, Journet E-P, de Carvalho-Niebel F, Duc G, Frugoli J**. 2005. The Medicago truncatula SUNN gene encodes a CLV1-like leucine-rich repeat receptor kinase that regulates nodule number and root length. Plant molecular biology **58**, 809–822.

**Schnabel E, Karve A, Kassaw T, Mukherjee A, Zhou X, Hall T, Frugoli J**. 2012. The*M. truncatula SUNN*gene is expressed in vascular tissue, similarly to*RDN1*, consistent with the role of these nodulation regulation genes in long distance signaling. Plant signaling & behavior **7**, 4–6.

**Scott T, Correa-Lozano A, Foo E**. 2024. Upstairs, Downstairs - conserved and divergent CLAVATA signalling in shoot meristem development and root symbioses. Annals of botany doi: 10.1093/aob/mcae192.

**Searle IR, Men AE, Laniya TS, Buzas DM, Iturbe-Ormaetxe I, Carroll BJ, Gresshoff PM**. 2003. Long-distance signaling in nodulation directed by a CLAVATA1-like receptor kinase. Science **299**, 109–112.

**Selby R, Jones DS**. 2023. Complex peptide hormone signaling in plant stem cells. Current opinion in plant biology **75**, 102442.

**Serrano K, Bezrutczyk M, Goudeau D, Dao T, O'Malley R, Malmstrom RR, Visel A, Scheller HV, Cole B**. 2024. Spatial co-transcriptomics reveals discrete stages of the arbuscular mycorrhizal symbiosis. Nature plants **10**, 673–688.

**Smit P, Limpens E, Geurts R, Fedorova E, Dolgikh E, Gough C, Bisseling T**. 2007. Medicago LYK3, an entry receptor in rhizobial nodulation factor signaling. Plant physiology **145**, 183–191.

**Smith SE, Reid D**. 2008. *Mycorrhizal Symbiosis*. Academic Press.

**Somssich M, Bleckmann A, Simon R**. 2016*a*. Shared and distinct functions of the pseudokinase CORYNE (CRN) in shoot and root stem cell maintenance of Arabidopsis. Journal of experimental botany **67**, 4901–4915.

**Somssich M, Je BI, Simon R, Jackson D**. 2016*b*. CLAVATA-WUSCHEL signaling in the shoot meristem. Development **143**, 3238–3248.

**Stahl Y, Grabowski S, Bleckmann A, *et al.*** 2013. Moderation of Arabidopsis root stemness by CLAVATA1 and ARABIDOPSIS CRINKLY4 receptor kinase complexes. Current biology: CB **23**, 362–371.

**Stammers DK**. 2001. The structure of the negative transcriptional regulator NmrA reveals a structural superfamily which includes the short-chain dehydrogenase/reductases. The EMBO journal **20**, 6619–6626.

**Tang H, Krishnakumar V, Bidwell S, *et al.*** 2014. An improved genome release (version Mt4.0) for the model legume Medicago truncatula. BMC genomics **15**, 312.

**Thomas J, Frugoli J**. 2024. Mutation of BAM2 rescues the sunn hypernodulation phenotype in Medicago truncatula, suggesting that a signaling pathway like CLV1/BAM in Arabidopsis affects nodule number. Frontiers in plant science **14**.

**Tian C, Kasiborski B, Koul R, Lammers PJ, Bücking H, Shachar-Hill Y**. 2010. Regulation of the nitrogen transfer pathway in the arbuscular mycorrhizal symbiosis: Gene characterization and the coordination of expression with nitrogen flux. Plant physiology **153**, 1175–1187.

**Torres Ascurra YC, Müller LM**. 2025. Signaling peptides control beneficial and pathogenic plant-microbe interactions. Journal of experimental botany, eraf180.

**Tsuno Y, Fujimatsu T, Endo K, Sugiyama A, Yazaki K**. 2018. Soyasaponins: A New Class of Root Exudates in Soybean (Glycine max). Plant & cell physiology **59**, 366–375.

**Vicente J, Cascón T, Vicedo B, García-Agustín P, Hamberg M, Castresana C**. 2012. Role of 9-lipoxygenase and α-dioxygenase oxylipin pathways as modulators of local and systemic defense. Molecular plant **5**, 914–928.

**Wang C, Reid JB, Foo E**. 2018. The Art of Self-Control - Autoregulation of Plant-Microbe Symbioses. Frontiers in plant science **9**, 988.

**Wang C, Velandia K, Kwon C-T, Wulf KE, Nichols DS, Reid JB, Foo E**. 2021. The role of CLAVATA signalling in the negative regulation of mycorrhizal colonization and nitrogen response of tomato. Journal of experimental botany **72**, 1702–1713.

**Whitewoods CD**. 2021. Evolution of CLE peptide signalling. Seminars in cell & developmental biology **109**, 12–19.

**Wojtaszek P**. 1997. Oxidative burst: an early plant response to pathogen infection. The Biochemical journal **322**, 681–692.

**Wulf K, Sun J, Wang C, *et al.*** 2024. The role of CLE peptides in the suppression of mycorrhizal colonization of tomato. Plant & cell physiology **65**, 107–119.

**Xie X, Lai W, Che X, Wang S, Ren Y, Hu W, Chen H, Tang M**. 2022. A SPX domain-containing phosphate transporter from *Rhizophagus irregularis* handles phosphate homeostasis at symbiotic interface of arbuscular mycorrhizas. The new phytologist **234**, 650–671.

**Xie Z, Nolan TM, Jiang H, Yin Y**. 2019. AP2/ERF transcription factor regulatory networks in hormone and abiotic stress responses in Arabidopsis. Frontiers in plant science **10**.

**Yildirir G, Sperschneider J, Malar C M, Chen ECH, Iwasaki W, Cornell C, Corradi N**. 2022. Long reads and Hi-C sequencing illuminate the two-compartment genome of the model arbuscular mycorrhizal symbiont *Rhizophagus irregularis*. The new phytologist **233**, 1097–1107.

**Yoneyama K, Xie X, Kim HI, Kisugi T, Nomura T, Sekimoto H, Yokota T, Yoneyama K**. 2012. How do nitrogen and phosphorus deficiencies affect strigolactone production and exudation? Planta **235**, 1197–1207.

**Yoneyama K, Xie X, Kusumoto D, Sekimoto H, Sugimoto Y, Takeuchi Y, Yoneyama K**. 2007. Nitrogen deficiency as well as phosphorus deficiency in sorghum promotes the production and exudation of 5-deoxystrigol, the host recognition signal for arbuscular mycorrhizal fungi and root parasites. Planta **227**, 125–132.

**Zhang J, Sun J, Chiu CH, *et al.*** 2024. A receptor required for chitin perception facilitates arbuscular mycorrhizal associations and distinguishes root symbiosis from immunity. Current biology: CB **34**, 1705-1717.e6.